



# Accident Analysis

One of the central purposes of this investigation, like those for other kinds of accidents, was to identify the chain of circumstances that caused the *Columbia* accident. In this case the task was particularly challenging, because the breakup of the Orbiter occurred at hypersonic velocities and extremely high altitudes, and the debris was scattered over a wide area. Moreover, the initiating event preceded the accident by more than two weeks. In pursuit of the sequence of the cause, investigators developed a broad array of information sources. Evidence was derived from film and video of the launch, radar images of *Columbia* on orbit, and amateur video of debris shedding during the in-flight breakup. Data was obtained from sensors onboard the Orbiter – some of this data was downlinked during the flight, and some came from an on-board recorder that was recovered during the debris search. Analysis of the debris was particularly valuable to the investigation. Clues were to be found not only in the condition of the pieces, but also in their location – both where they had been on the Orbiter and where they were found on the ground. The investigation also included extensive computer modeling, impact tests, wind tunnel studies, and other analytical techniques. Each of these avenues of inquiry is described in this chapter.

Because it became evident that the key event in the chain leading to the accident involved both the External Tank and one of the Orbiter's wings, the chapter includes a study of these two structures. The understanding of the accident's physical cause that emerged from this investigation is summarized in the statement at the beginning of the chapter. Included in the chapter are the findings and recommendations of the Columbia Accident Investigation Board that are based on this examination of the physical evidence.

## 3.1 THE PHYSICAL CAUSE

The physical cause of the loss of *Columbia* and its crew was a breach in the Thermal Protection System on the leading edge of the left wing. The breach was initiated by a piece of insulating foam that separated from the left bipod ramp of the External Tank and struck the wing in the vicinity of the lower half of Reinforced Carbon-Carbon panel 8 at 81.9 seconds after launch. During re-entry, this breach in the Thermal

Protection System allowed superheated air to penetrate the leading-edge insulation and progressively melt the aluminum structure of the left wing, resulting in a weakening of the structure until increasing aerodynamic forces caused loss of control, failure of the wing, and breakup of the Orbiter.



Figure 3.1-1. Columbia sitting at Launch Complex 39-A. The upper circle shows the left bipod (-Y) ramp on the forward attach point, while the lower circle is around RCC panel 8-left.

### 3.2 THE EXTERNAL TANK AND FOAM

The External Tank is the largest element of the Space Shuttle. Because it is the common element to which the Solid Rocket Boosters and the Orbiter are connected, it serves as the main structural component during assembly, launch, and ascent. It also fulfills the role of the low-temperature, or cryogenic, propellant tank for the Space Shuttle Main Engines. It holds 143,351 gallons of liquid oxygen at minus 297 degrees Fahrenheit in its forward (upper) tank and 385,265 gallons of liquid hydrogen at minus 423 degrees Fahrenheit in its aft (lower) tank.<sup>1</sup>

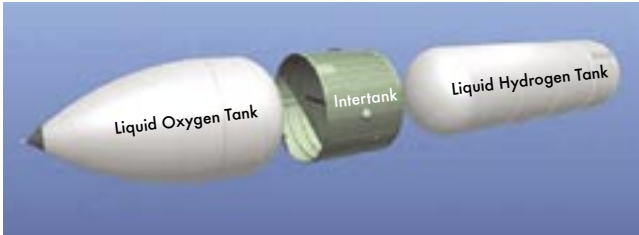


Figure 3.2-1. The major components of the External Tank.

Lockheed Martin builds the External Tank under contract to the NASA Marshall Space Flight Center at the Michoud Assembly Facility in eastern New Orleans, Louisiana.

The External Tank is constructed primarily of aluminum alloys (mainly 2219 aluminum alloy for standard-weight and lightweight tanks, and 2195 Aluminum-Lithium alloy for super-lightweight tanks), with steel and titanium fittings and attach points, and some composite materials in fairings and access panels. The External Tank is 153.8 feet long and 27.6 feet in diameter, and comprises three major sections: the liquid oxygen tank, the liquid hydrogen tank, and the intertank area between them (see Figure 3.2-1). The liquid oxygen and liquid hydrogen tanks are welded assemblies of machined and formed panels, barrel sections, ring frames, and dome and ogive sections. The liquid oxygen tank is pressure-tested with water, and the liquid hydrogen tank with compressed air, before they are incorporated into the External Tank assembly. STS-107 used Lightweight External Tank-93.

The propellant tanks are connected by the intertank, a 22.5-foot-long hollow cylinder made of eight stiffened aluminum alloy panels bolted together along longitudinal joints. Two of these panels, the integrally stiffened thrust panels (so called because they react to the Solid Rocket Booster thrust loads) are located on the sides of the External Tank where the Solid Rocket Boosters are mounted; they consist of single slabs of aluminum alloy machined into panels with solid longitudinal ribs. The thrust panels are joined across the inner diameter by the intertank truss, the major structural element of the External Tank. During propellant loading, nitrogen is used to purge the intertank to prevent condensation and also to prevent liquid oxygen and liquid hydrogen from combining.

The External Tank is attached to the Solid Rocket Boosters by bolts and fittings on the thrust panels and near the aft end of the liquid hydrogen tank. The Orbiter is attached to the Ex-

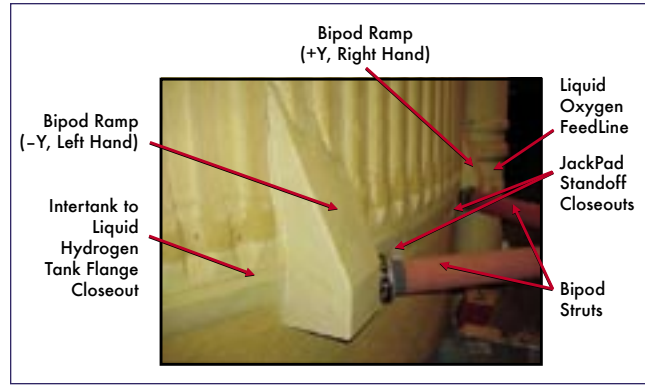


Figure 3.2-2. The exterior of the left bipod attachment area showing the foam ramp that came off during the ascent of STS-107.

ternal Tank by two umbilical fittings at the bottom (that also contain fluid and electrical connections) and by a “bipod” at the top. The bipod is attached to the External Tank by fittings at the right and left of the External Tank centerline. The bipod fittings, which are titanium forgings bolted to the External Tank, are forward (above) of the intertank-liquid hydrogen flange joint (see Figures 3.2-2 and 3.2-3). Each forging contains a spindle that attaches to one end of a bipod strut and rotates to compensate for External Tank shrinkage during the loading of cryogenic propellants.

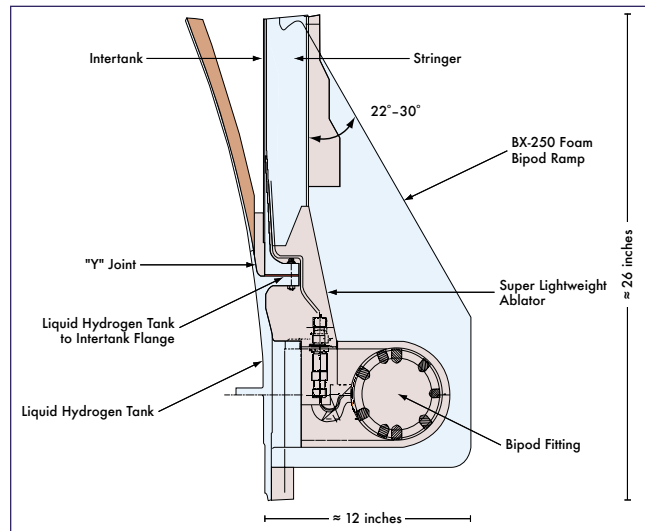


Figure 3.2-3. Cutaway drawing of the bipod ramp and its associated fittings and hardware.

#### External Tank Thermal Protection System Materials

The External Tank is coated with two materials that serve as the Thermal Protection System: dense composite ablators for dissipating heat, and low density closed-cell foams for high insulation efficiency.<sup>2</sup> (Closed-cell materials consist of small pores filled with air and blowing agents that are separated by thin membranes of the foam’s polymeric component.) The External Tank Thermal Protection System is designed to maintain an interior temperature that keeps the

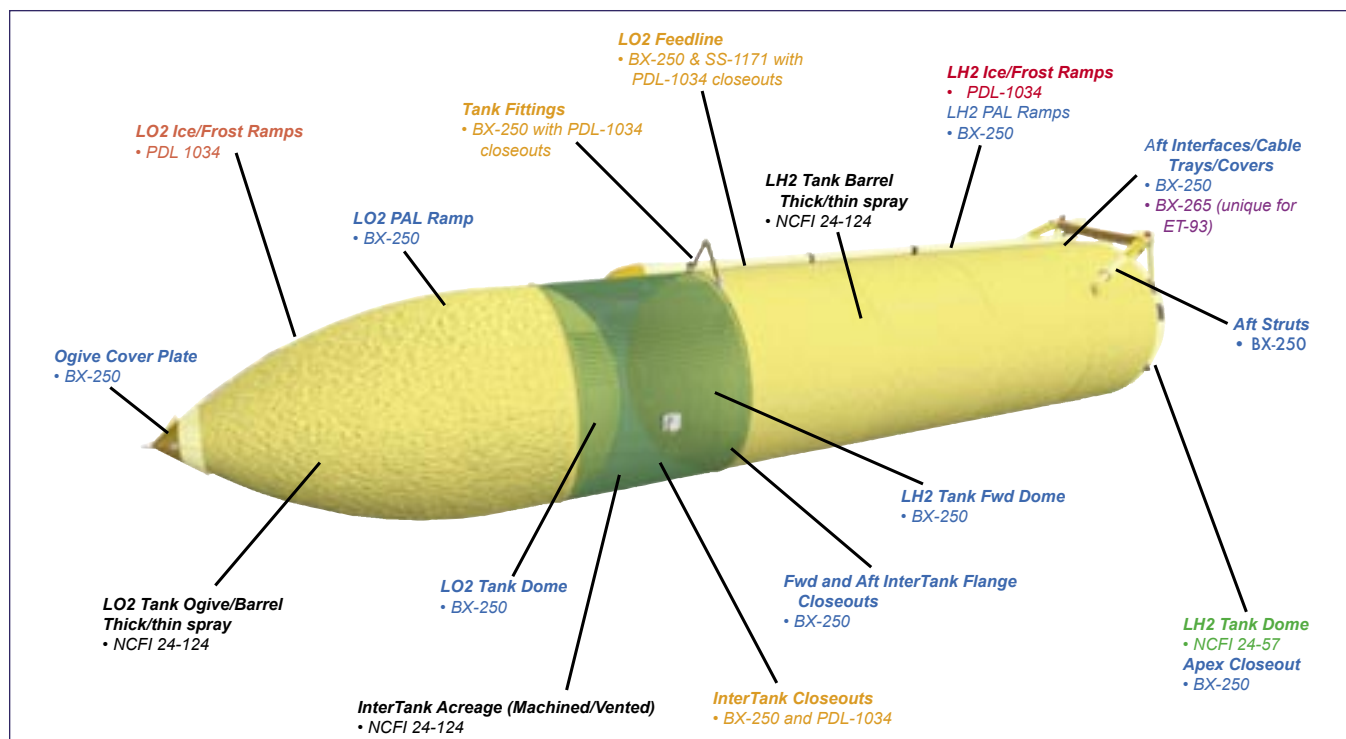


Figure 3.2-4. Locations of the various foam systems as used on ET-93, the External Tank used for STS-107.

oxygen and hydrogen in a liquid state, and to maintain the temperature of external parts high enough to prevent ice and frost from forming on the surface. Figure 3.2-4 summarizes the foam systems used on the External Tank for STS-107.

The adhesion between sprayed-on foam insulation and the External Tank's aluminum substrate is actually quite good, provided that the substrate has been properly cleaned and primed. (Poor surface preparation does not appear to have been a problem in the past.) In addition, large areas of the aluminum substrate are usually heated during foam application to ensure that the foam cures properly and develops the maximum adhesive strength. The interface between the foam and the aluminum substrate experiences stresses due to differences in how much the aluminum and the foam contract when subjected to cryogenic temperatures, and due to the stresses on the External Tank's aluminum structure while it serves as the backbone of the Shuttle stack. While these stresses at the foam-aluminum interface are certainly not trivial, they do not appear to be excessive, since very few of the observed foam loss events indicated that the foam was lost down to the primed aluminum substrate.

Throughout the history of the External Tank, factors unrelated to the insulation process have caused foam chemistry changes (Environmental Protection Agency regulations and material availability, for example). The most recent changes resulted from modifications to governmental regulations of chlorofluorocarbons.

Most of the External Tank is insulated with three types of spray-on foam. NCFI 24-124, a polyisocyanurate foam applied with blowing agent HCFC 141b hydrochlorofluorocar-

bon, is used on most areas of the liquid oxygen and liquid hydrogen tanks. NCFI 24-57, another polyisocyanurate foam applied with blowing agent HCFC 141b hydrochlorofluorocarbon, is used on the lower liquid hydrogen tank dome. BX-250, a polyurethane foam applied with CFC-11 chlorofluorocarbon, was used on domes, ramps, and areas where the foam is applied by hand. The foam types changed on External Tanks built after External Tank 93, which was used on STS-107, but these changes are beyond the scope of this section.

Metallic sections of the External Tank that will be insulated with foam are first coated with an epoxy primer. In some areas, such as on the bipod hand-sculpted regions, foam is applied directly over ablator materials. Where foam is applied over cured or dried foam, a bonding enhancer called Conathane is first applied to aid the adhesion between the two foam coats.

After foam is applied in the intertank region, the larger areas of foam coverage are machined down to a thickness of about an inch. Since controlling weight is a major concern for the External Tank, this machining serves to reduce foam thickness while still maintaining sufficient insulation.

The insulated region where the bipod struts attach to the External Tank is structurally, geometrically, and materially complex. Because of concerns that foam applied over the fittings would not provide enough protection from the high heating of exposed surfaces during ascent, the bipod fittings are coated with ablators. BX-250 foam is sprayed by hand over the fittings (and ablator materials), allowed to dry, and manually shaved into a ramp shape. The foam is visually

inspected at the Michoud Assembly Facility and also at the Kennedy Space Center, but no other non-destructive evaluation is performed.

Since the Shuttle's inaugural flight, the shape of the bipod ramp has changed twice. The bipod foam ramps on External Tanks 1 through 13 originally had a 45-degree ramp angle. On STS-7, foam was lost from the External Tank bipod ramp; subsequent wind tunnel testing showed that shallower angles were aerodynamically preferable. The ramp angle was changed from 45 degrees to between 22 and 30 degrees on External Tank 14 and later tanks. A slight modification to the ramp impingement profile, implemented on External Tank 76 and later, was the last ramp geometry change.

### STS-107 Left Bipod Foam Ramp Loss

A combination of factors, rather than a single factor, led to the loss of the left bipod foam ramp during the ascent of STS-107. NASA personnel believe that testing conducted during the investigation, including the dissection of as-built hardware and testing of simulated defects, showed conclusively that pre-existing defects in the foam were a major factor, and in briefings to the Board, these were cited as a necessary condition for foam loss. However, analysis indicated that pre-existing defects alone were not responsible for foam loss.

The basic External Tank was designed more than 30 years ago. The design process then was substantially different than it is today. In the 1970s, engineers often developed particular facets of a design (structural, thermal, and so on) one after another and in relative isolation from other engineers working on different facets. Today, engineers usually work together on all aspects of a design as an integrated team. The bipod fitting was designed first from a structural standpoint, and the application processes for foam (to prevent ice formation) and Super Lightweight Ablator (to protect from high heating) were developed separately. Unfortunately, the structurally optimum fitting design, along with the geometric complexity of its location (near the flange between the intertank and the liquid hydrogen tank), posed many problems in the application of foam and Super Lightweight Ablator that would lead to foam-ramp defects.

Although there is no evidence that substandard methods were used to qualify the bipod ramp design, tests made nearly three decades ago were rudimentary by today's standards and capabilities. Also, testing did not follow the often-used engineering and design philosophy of "Fly what you test and test what you fly." Wind tunnel tests observed the aerodynamics and strength of two geometries of foam bipod enclosures (flat-faced and a 20-degree ramp), but these tests were done on essentially solid foam blocks that were not sprayed onto the complex bipod fitting geometry. Extensive material property tests gauged the strength, insulating potential, and ablative characteristics of foam and Super Lightweight Ablator specimens.

It was – and still is – impossible to conduct a ground-based, simultaneous, full-scale simulation of the combination of loads, airflows, temperatures, pressures, vibration, and acoustics the External Tank experiences during launch and

ascent. Therefore, the qualification testing did not truly reflect the combination of factors the bipod would experience during flight. Engineers and designers used the best methods available at the time: test the bipod and foam under as many severe combinations as could be simulated and then interpolate the results. Various analyses determined stresses, thermal gradients, air loads, and other conditions that could not be obtained through testing.

Significant analytical advancements have been made since the External Tank was first conceived, particularly in computational fluid dynamics (see Figure 3.2-5). Computational fluid dynamics comprises a computer-generated model that represents a system or device and uses fluid-flow physics and software to create predictions of flow behavior, and stress or deformation of solid structures. However, analysis must always be verified by test and/or flight data. The External Tank and the bipod ramp were not tested in the complex flight environment, nor were fully instrumented External Tanks ever launched to gather data for verifying analytical tools. The accuracy of the analytical tools used to simulate the External Tank and bipod ramp were verified only by using flight and test data from other Space Shuttle regions.

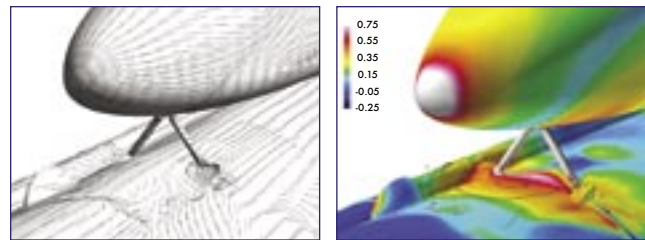


*Figure 3.2-5. Computational Fluid Dynamics was used to understand the complex flow fields and pressure coefficients around bipod strut. The flight conditions shown here approximate those present when the left bipod foam ramp was lost from External Tank 93 at Mach 2.46 at a 2.08-degree angle of attack.*

Further complicating this problem, foam does not have the same properties in all directions, and there is also variability in the foam itself. Because it consists of small hollow cells, it does not have the same composition at every point. This combination of properties and composition makes foam extremely difficult to model analytically or to characterize physically. The great variability in its properties makes for difficulty in predicting its response in even relatively static conditions, much less during the launch and ascent of the Shuttle. And too little effort went into understanding the origins of this variability and its failure modes.

The way the foam was produced and applied, particularly in the bipod region, also contributed to its variability. Foam consists of two chemical components that must be mixed in an exact ratio and is then sprayed according to strict specifications. Foam is applied to the bipod fitting by hand to make the foam ramp, and this process may be the primary source of foam variability. Board-directed dissection of foam ramps has revealed that defects (voids, pockets, and debris) are likely due to a lack of control of various combinations of parameters in spray-by-hand applications, which

is exacerbated by the complexity of the underlying hardware configuration. These defects often occur along “knit lines,” the boundaries between each layer that are formed by the repeated application of thin layers – a detail of the spray-by-hand process that contributes to foam variability, suggesting that while foam is sprayed according to approved procedures, these procedures may be questionable if the people who devised them did not have a sufficient understanding of the properties of the foam.

Subsurface defects can be detected only by cutting away the foam to examine the interior. Non-destructive evaluation techniques for determining External Tank foam strength have not been perfected or qualified (although non-destructive testing has been used successfully on the foam on Boeing’s new Delta IV booster, a design of much simpler geometry than the External Tank). Therefore, it has been impossible to determine the quality of foam bipod ramps on any External Tank. Furthermore, multiple defects in some cases can combine to weaken the foam along a line or plane.

“Cryopumping” has long been theorized as one of the processes contributing to foam loss from larger areas of coverage. If there are cracks in the foam, and if these cracks lead through the foam to voids at or near the surface of the liquid oxygen and liquid hydrogen tanks, then air, chilled by the extremely low temperatures of the cryogenic tanks, can liquefy in the voids. After launch, as propellant levels fall and aerodynamic heating of the exterior increases, the temperature of the trapped air can increase, leading to boiling and evaporation of the liquid, with concurrent buildup of pressure within the foam. It was believed that the resulting rapid increase in subsurface pressure could cause foam to break away from the External Tank.

“Cryoingestion” follows essentially the same scenario, except it involves gaseous nitrogen seeping out of the intertank and liquefying inside a foam void or collecting in the Super Lightweight Ablator. (The intertank is filled with nitrogen during tanking operations to prevent condensation and also to prevent liquid hydrogen and liquid oxygen from combining.) Liquefying would most likely occur in the circumferential “Y” joint, where the liquid hydrogen tank mates with the intertank, just above the liquid hydrogen-intertank flange. The bipod foam ramps straddle this complex feature. If pooled liquid nitrogen contacts the liquid hydrogen tank, it can solidify, because the freezing temperature of liquid nitrogen (minus 348 degrees Fahrenheit) is higher than the temperature of liquid hydrogen (minus 423 degrees Fahrenheit). As with cryopumping, cryoingested liquid or solid nitrogen could also “flash evaporate” during launch and ascent, causing the foam to crack off. Several paths allow gaseous nitrogen to escape from the intertank, including beneath the flange, between the intertank panels, through the rivet holes that connect stringers to intertank panels, and through vent holes beneath the stringers that prevent overpressurization of the stringers.

No evidence suggests that defects or cryo-effects alone caused the loss of the left bipod foam ramp from the STS-107 External Tank. Indeed, NASA calculations have suggested that during ascent, the Super Lightweight Ablator

remains just slightly above the temperature at which nitrogen liquefies, and that the outer wall of the hydrogen tank near the bipod ramp does not reach the temperature at which nitrogen boils until 150 seconds into the flight,<sup>3</sup> which is too late to explain the only two bipod ramp foam losses whose times during ascent are known. Recent tests at the Marshall Space Flight Center revealed that flight conditions could permit ingestion of nitrogen or air into subsurface foam, but would not permit “flash evaporation” and a sufficient subsurface pressure increase to crack the foam. When conditions are modified to force a flash evaporation, the failure mode in the foam is a crack that provides pressure relief rather than explosive cracking. Therefore, the flight environment itself must also have played a role. Aerodynamic loads, thermal and vacuum effects, vibrations, stress in the External Tank structure, and myriad other conditions may have contributed to the growth of subsurface defects, weakening the foam ramp until it could no longer withstand flight conditions.

Conditions in certain combinations during ascent may also have contributed to the loss of the foam ramp, even if individually they were well within design certification limits. These include a wind shear, associated Solid Rocket Booster and Space Shuttle Main Engine responses, and liquid oxygen sloshing in the External Tank.<sup>4</sup> Each of these conditions, alone, does not appear to have caused the foam loss, but their contribution to the event in combination is unknown.

Negligence on the part of NASA, Lockheed Martin, or United Space Alliance workers does not appear to have been a factor. There is no evidence of sabotage, either during production or pre-launch. Although a Problem Report was written for a small area of crushed foam near the left bipod (a condition on nearly every flight), this affected only a very small region and does not appear to have contributed to the loss of the ramp (see Chapter 4 for a fuller discussion). Nor does the basic quality of the foam appear to be a concern. Many of the basic components are continually and meticulously tested for quality before they are applied. Finally, despite commonly held perceptions, numerous tests show that moisture absorption and ice formation in the foam appears negligible.

Foam loss has occurred on more than 80 percent of the 79 missions for which imagery is available, and foam was lost from the left bipod ramp on nearly 10 percent of missions where the left bipod ramp was visible following External Tank separation. For about 30 percent of all missions, there is no way to determine if foam was lost; these were either night launches, or the External Tank bipod ramp areas were not in view when the images were taken. The External Tank was not designed to be instrumented or recovered after separation, which deprives NASA of physical evidence that could help pinpoint why foam separates from it.

The precise reasons why the left bipod foam ramp was lost from the External Tank during STS-107 may never be known. The specific initiating event may likewise remain a mystery. However, it is evident that a combination of variable and pre-existing factors, such as insufficient testing and analysis in the early design stages, resulted in a highly variable and complex foam material, defects induced by an imperfect

## FOAM FRACTURE UNDER HYDROSTATIC PRESSURE

The Board has concluded that the physical cause of the breakup of *Columbia* upon re-entry was the result of damage to the Orbiter's Thermal Protection System, which occurred when a large piece of BX-250 foam insulation fell from the left (-Y) bipod assembly 81.7 seconds after launch and struck the leading edge of the left wing. As the External Tank is covered with insulating foam, it seemed to me essential that we understand the mechanisms that could cause foam to shed.

Many if not most of the systems in the three components of the Shuttle stack (Orbiter, External Tank, and Solid Rocket Boosters) are by themselves complex, and often operate near the limits of their performance. Attempts to understand their complex behavior and failure modes are hampered by their strong interactions with other systems in the stack, through their shared environment. The foam of the Thermal Protection System is no exception. To understand the behavior of systems under such circumstances, one must first understand their behavior in relatively simple limits. Using this understanding as a guide, one is much more likely to determine the mechanisms of complex behavior, such as the shedding of foam from the -Y bipod ramp, than simply creating simulations of the complex behavior itself.

I approached this problem by trying to imagine the fracture mechanism by which fluid pressure built up inside the foam could propagate to the surface. Determining this process is clearly key to understanding foam ejection through the heating of cryogenic fluids trapped in voids beneath the surface of the foam, either through "cryopumping" or "cryoingestion." I started by imagining a fluid under hydrostatic pressure in contact with the surface of such foam. It seemed clear that as the pressure increased, it would cause the weakest cell wall to burst, filling the adjacent cell with the fluid, and exerting the same hydrostatic pressure on all the walls of that cell. What happened next was unclear. It was possible that the next cell wall to burst would not be one of the walls of the newly filled cell, but some other cell that had been on the surface that was initially subjected to the fluid pressure. This seemed like a rather complex process, and I questioned my ability to include all the physics correctly if I tried to model it. Instead, I chose to perform an experiment that seemed straightforward, but which had a result I could not have foreseen.

I glued a 1.25-inch-thick piece of BX-250 foam to a 0.25-inch-thick brass plate. The 3-by-3-inch plate had a 0.25-inch-diameter hole in its center, into which a brass tube was soldered. The tube was filled with a liquid dye, and the air pressure above the dye could be slowly raised, using a battery-operated tire pump to which a pressure regulator was attached until the fluid was forced through the foam to its outer surface. Not knowing what to expect, the first time I tried this experiment with my graduate student, Jim Baumgardner, we did so out on the loading dock of the Stanford Physics Department. If this process were to mimic the cryoejection of foam, we expected a violent explosion when the pressure burst through the surface. To keep from being showered with dye, we put the assembly in a closed cardboard box, and donned white lab coats.

Instead of a loud explosion, we heard nothing. We found, though, that the pressure above the liquid began dropping once the gas pressure reached about 45 pounds per square inch. Releasing the pressure and opening the box, we found a thin crack, about a half-inch long, at the upper surface of the foam. Curious about the path the pressure had taken to reach the surface, I cut the foam off the brass plate, and made two vertical cuts through the foam in line with the crack. When I bent the foam in line with the crack, it separated into two sections along the crack. The dye served as a tracer for where the fluid had traveled in its path through the foam. This path was along a flat plane, and was

the shape of a teardrop that intersected perpendicular to the upper surface of the foam. Since the pressure could only exert force in the two directions perpendicular to this fault plane, it could not possibly result in the ejection of foam, because that would require a force perpendicular to the surface of the foam. I repeated this experiment with several pieces of foam and always found the same behavior.

I was curious why the path of the pressure fault was planar, and why it had propagated upward, nearly perpendicular to the outer surface of the foam. For this sample, and most of the samples that NASA had given me, the direction of growth of the foam was vertical, as evidenced by horizontal "knit lines" that result from successive applications of the sprayed foam. The knit lines are perpendicular to the growth direction. I then guessed that the growth of the pressure fault was influenced by the foam's direction of growth. To test this hypothesis, I found a piece of foam for which the growth direction was vertical near the top surface of the foam, but was at an approximately 45-degree angle to the vertical near the bottom. If my hypothesis were correct, the direction of growth of the pressure fault would follow the direction of growth of the foam, and hence would always intersect the knit lines at 90 degrees. Indeed, this was the case.

The reason the pressure fault is planar has to do with the fact that such a geometry can amplify the fluid pressure, creating a much greater stress on the cell walls near the outer edges of the teardrop, for a given hydrostatic pressure, than would exist for a spherical pressure-filled void. A pressure fault follows the direction of foam growth because more cell walls have their surfaces along this direction than along any other. The stiffness of the foam is highest when you apply a force parallel to the cell walls. If you squeeze a cube of foam in various directions, you find that the foam is stiffest along its growth direction. By advancing along the stiff direction, the crack is oriented so that the fluid pressure can more easily force the (nearly) planar walls of the crack apart.

Because the pressure fault intersects perpendicular to the upper surface, hydrostatic pressure will *generally* not lead to foam shedding. There are, however, cases where pressure *can* lead to foam shedding, but this will only occur when the fluid pressure exists over an area whose dimensions are large compared to the thickness of the foam above it, and roughly parallel to the outer surface. This would require a large structural defect within the foam, such as the delamination of the foam from its substrate or the separation of the foam at a knit line. Such large defects are quite different from the small voids that occur when gravity causes uncured foam to "roll over" and trap a small bubble of air.

Experiments like this help us understand how foam shedding does (and doesn't) occur, because they elucidate the properties of "perfect" foam, free from voids and other defects. Thus, this behavior represents the true behavior of the foam, free from defects that may or may not have been present. In addition, these experiments are fast and cheap, since they can be carried out on relatively small pieces of foam in simple environments. Finally, we can understand why the observed behavior occurs from our understanding of the basic physical properties of the foam itself. By contrast, if you wish to mimic left bipod foam loss, keep in mind that such loss could have been detected only 7 times in 72 instances. Thus, not observing foam loss in a particular experiment will not insure that it would never happen under the same conditions at a later time. NASA is now undertaking both kinds of experiments, but it is the simple studies that so far have most contributed to our understanding of foam failure modes.

*Douglas Osheroff, Board Member*

and variable application, and the results of that imperfect process, as well as severe load, thermal, pressure, vibration, acoustic, and structural launch and ascent conditions.

**Findings:**

- F3.2-1 NASA does not fully understand the mechanisms that cause foam loss on almost all flights from larger areas of foam coverage and from areas that are sculpted by hand.
- F3.2-2 There are no qualified non-destructive evaluation techniques for the as-installed foam to determine the characteristics of the foam before flight.
- F3.2-3 Foam loss from an External Tank is unrelated to the tank's age and to its total pre-launch exposure to the elements. Therefore, the foam loss on STS-107 is unrelated to either the age or exposure of External Tank 93 before launch.
- F3.2-4 The Board found no indications of negligence in the application of the External Tank Thermal Protection System.
- F3.2-5 The Board found instances of left bipod ramp shedding on launch that NASA was not aware of, bringing the total known left bipod ramp shedding events to 7 out of 72 missions for which imagery of the launch or External Tank separation is available.
- F3.2-6 Subsurface defects were found during the dissection of three bipod foam ramps, suggesting that similar defects were likely present in the left bipod ramp of External Tank 93 used on STS-107.
- F3.2-7 Foam loss occurred on more than 80 percent of the 79 missions for which imagery was available to confirm or rule out foam loss.
- F3.2-8 Thirty percent of all missions lacked sufficient imagery to determine if foam had been lost.
- F3.2-9 Analysis of numerous separate variables indicated that none could be identified as the sole initiating factor of bipod foam loss. The Board therefore concludes that a combination of several factors resulted in bipod foam loss.

**Recommendation:**

- R3.2-1 Initiate an aggressive program to eliminate all External Tank Thermal Protection System debris-shedding at the source with particular emphasis on the region where the bipod struts attach to the External Tank.

**3.3 WING LEADING EDGE STRUCTURAL SUBSYSTEM**

The components of the Orbiter's wing leading edge provide the aerodynamic load bearing, structural, and thermal control capability for areas that exceed 2,300 degrees Fahrenheit. Key design requirements included flying 100 missions with minimal refurbishment, maintaining the aluminum wing structure at less than 350 degrees Fahrenheit, withstanding a kinetic energy impact of 0.006 foot-pounds, and the ability to withstand 1.4 times the load ever expected in operation.<sup>5</sup> The requirements specifically stated that the

**REINFORCED CARBON-CARBON (RCC)**

The basic RCC composite is a laminate of graphite-impregnated rayon fabric, further impregnated with phenolic resin and layered, one ply at a time, in a unique mold for each part, then cured, rough-trimmed, drilled, and inspected. The part is then packed in calcined coke and fired in a furnace to convert it to carbon and is made more dense by three cycles of furfuryl alcohol vacuum impregnation and firing.

To prevent oxidation, the outer layers of the carbon substrate are converted into a 0.02-to-0.04-inch-thick layer of silicon carbide in a chamber filled with argon at temperatures up to 3,000 degrees Fahrenheit. As the silicon carbide cools, "craze cracks" form because the thermal expansion rates of the silicon carbide and the carbon substrate differ. The part is then repeatedly vacuum-impregnated with tetraethyl orthosilicate to fill the pores in the substrate, and the craze cracks are filled with a sealant.

wing leading edge would not need to withstand impact from debris or ice, since these objects would not pose a threat during the launch phase.<sup>6</sup>

**Reinforced Carbon-Carbon**

The development of Reinforced Carbon-Carbon (RCC) as part of the Thermal Protection System was key to meeting the wing leading edge design requirements. Developed by Ling-Temco-Vought (now Lockheed Martin Missiles and Fire Control), RCC is used for the Orbiter nose cap, chin panel, forward External Tank attachment point, and wing leading edge panels and T-seals. RCC is a hard structural material, with reasonable strength across its operational temperature range (minus 250 degrees Fahrenheit to 3,000 degrees). Its low thermal expansion coefficient minimizes thermal shock and thermoelastic stress.

Each wing leading edge consists of 22 RCC panels (see Figure 3.3-1), numbered from 1 to 22 moving outward on each wing (the nomenclature is "5-left" or "5-right" to differentiate, for example, the two number 5 panels). Because the shape of the wing changes from inboard to outboard, each panel is unique.

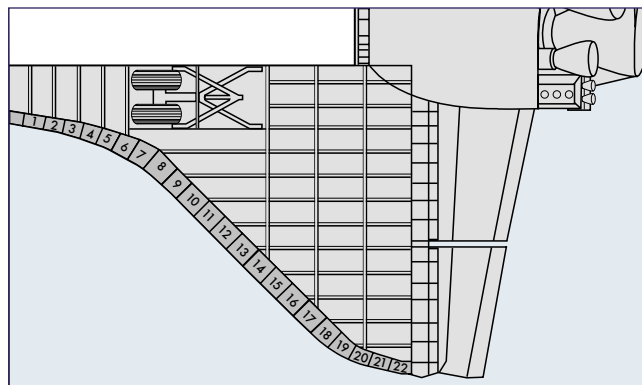


Figure 3.3-1. There are 22 panels of Reinforced Carbon-Carbon on each wing, numbered as shown above.

## Wing Leading Edge Damage

The risk of micrometeoroid or debris damage to the RCC panels has been evaluated several times. Hypervelocity impact testing, using nylon, glass, and aluminum projectiles, as well as low-velocity impact testing with ice, aluminum, steel, and lead projectiles, resulted in the addition of a 0.03- to 0.06-inch-thick layer of Nextel-440 fabric between the Inconel foil and Cerachrome insulation. Analysis of the design change predicts that the Orbiter could survive re-entry with a quarter-inch diameter hole in the lower surfaces of RCC panels 8 through 10 or with a one-inch hole in the rest of the RCC panels.

RCC components have been struck by objects throughout their operational life, but none of these components has been completely penetrated. A sampling of 21 post-flight reports noted 43 hypervelocity impacts, the largest being 0.2 inch. The most significant low-velocity impact was to *Atlantis*' panel 10-right during STS-45 in March and April 1992. The damaged area was 1.9 inches by 1.6 inches on the exterior surface and 0.5 inches by 0.1 inches in the interior surface. The substrate was exposed and oxidized, and the panel was scrapped. Analysis concluded that the damage was caused by a strike by a man-made object, possibly during ascent. Figures 3.3-2 and 3.3-3 show the damage to the outer and inner surfaces, respectively.

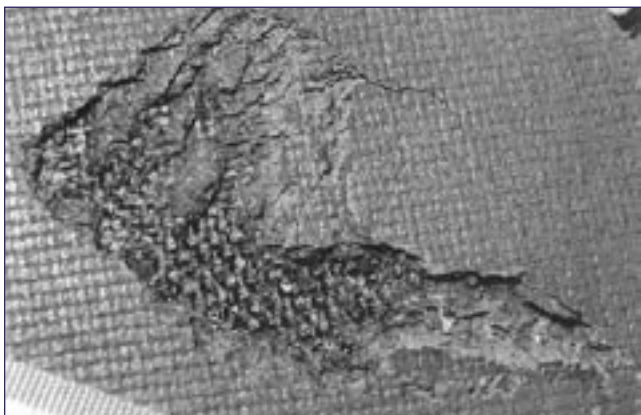


Figure 3.3-2. Damage on the outer surface of RCC panel 10-right from *Atlantis* after STS-45.

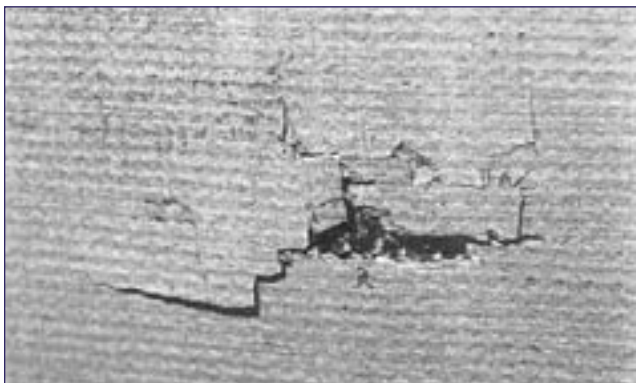


Figure 3.3-3. Damage on the inner surface of RCC panel 10-right from *Atlantis* after STS-45.

## Leading Edge Maintenance

Post-flight RCC component inspections for cracks, chips, scratches, pinholes, and abnormal discoloration are primarily visual, with tactile evaluations (pushing with a finger) of some regions. Boeing personnel at the Kennedy Space Center make minor repairs to the silicon carbide coating and surface defects.

With the goal of a long service life, panels 6 through 17 are refurbished every 18 missions, and panels 18 and 19 every 36 missions. The remaining panels have no specific refurbishment requirement.

At the time of STS-107, most of the RCC panels on *Columbia*'s left wing were original equipment, but panel 10-left, T-seal 10-left, panel 11-left, and T-seal 11-left had been replaced (along with panel 12 on the right wing). Panel 10-left was tested to destruction after 19 flights. Minor surface repairs had been made to panels 5, 7, 10, 11, 12, 13, and 19 and T-seals 3, 11, 12, 13, 14, and 19. Panels and T-seals 6 through 9 and 11 through 17 of the left wing had been refurbished.

## Reinforced Carbon-Carbon Mission Life

The rate of oxidation is the most important variable in determining the mission life of RCC components. Oxidation of the carbon substrate results when oxygen penetrates the microscopic pores or fissures of the silicon carbide protective coating. The subsequent loss of mass due to oxidation reduces the load the structure can carry and is the basis for establishing a mission life limit. The oxidation rate is a function of temperature, pressure, time, and the type of heating. Repeated exposure to the Orbiter's normal flight environment degrades the protective coating system and accelerates the loss of mass, which weakens components and reduces mission life capability.

Currently, mass loss of flown RCC components cannot be directly measured. Instead, mass loss and mission life reduction are predicted analytically using a methodology based on mass loss rates experimentally derived in simulated re-entry environments. This approach then uses derived re-entry temperature-time profiles of various portions of RCC components to estimate the actual re-entry mass loss.

For the first five missions of *Columbia*, the RCC components were not coated with Type A sealant, and had shorter mission service lives than the RCC components on the other Orbiters. (*Columbia*'s panel 9 has the shortest mission service life of 50 flights as shown in Figure 3.3-4.) The predicted life for panel/T-seals 7 through 16 range from 54 to 97 flights.<sup>7</sup>

Localized penetration of the protective coating on RCC components (pinholes) were first discovered on *Columbia* in 1992, after STS-50, *Columbia*'s 12th flight. Pinholes were later found in all Orbiters, and their quantity and size have increased as flights continue. Tests showed that pinholes were caused by zinc oxide contamination from a primer used on the launch pad.

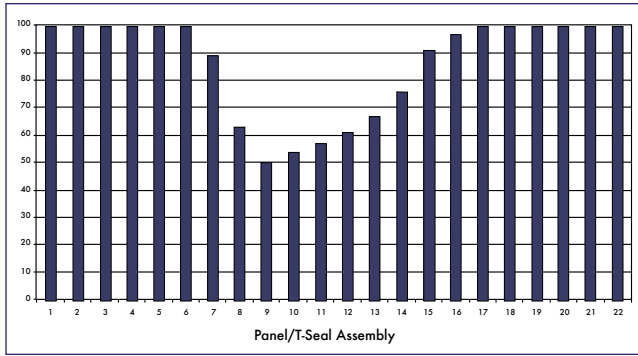


Figure 3.3-4. The expected mission life for each of the wing leading edge RCC panels on Columbia. Note that panel 9 has the shortest life expectancy.

In October 1993, panel 12-right was removed from *Columbia* after its 15th flight for destructive evaluation. Optical and scanning electron microscope examinations of 15 pinholes revealed that a majority occurred along craze cracks in the thick regions of the silicon carbide layer. Pinhole glass chemistry revealed the presence of zinc, silicon, oxygen, and aluminum. There is no zinc in the leading edge support system, but the launch pad corrosion protection system uses an inorganic zinc primer under a coat of paint, and this coat of paint is not always refurbished after a launch. Rain samples from the Rotating Support Structure at Launch Complex 39-A in July 1994 confirmed that rain washed the unprotected primer off the service structure and deposited it on RCC panels while the Orbiter sat on the launch pad. At the request of the Columbia Accident Investigation Board, rain samples were again collected in May 2003. The zinc

### LEFT WING AND WING LEADING EDGE

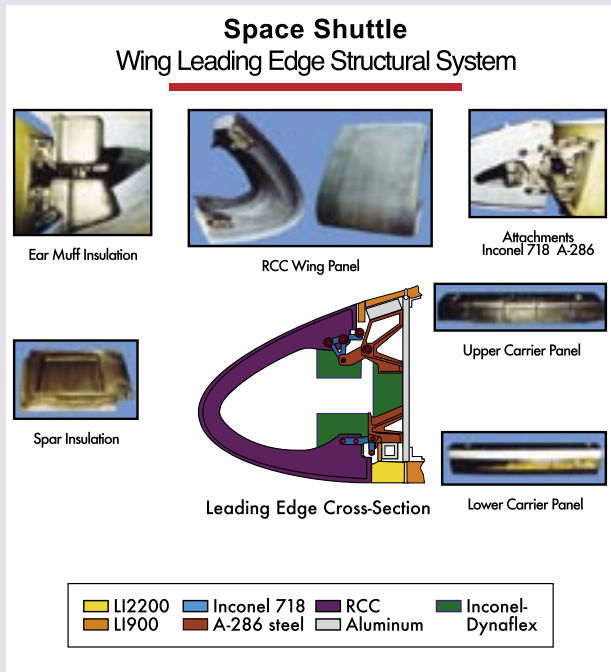
The Orbiter wing leading edge structural subsystem consists of the RCC panels, the upper and lower access panels (also called carrier panels), and the associated attachment hardware for each of these components.

On *Columbia*, two upper and lower A-286 stainless steel spar attachment fittings connected each RCC panel to the aluminum wing leading edge spar. On later Orbiters, each upper and lower spar attachment fitting is a one-piece assembly.

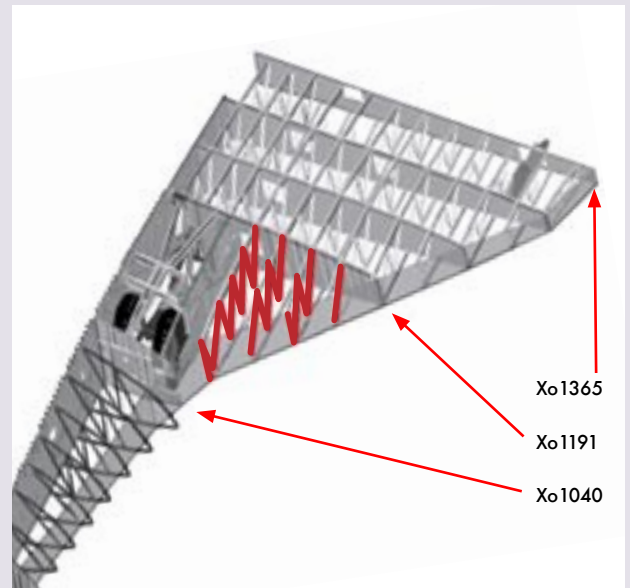
The space between each RCC panel is covered by a gap seal, also known as a T-seal. Each T-seal, also manufactured from RCC, is attached to its associated RCC panel by two Inconel 718 attachment clevises. The upper and lower carrier panels, which allow access behind each RCC panel, are attached to the spar attachment fittings after the RCC panels and T-seals are installed. The lower carrier panel prevents superheated air from entering

the RCC panel cavity. A small space between the upper carrier panel and the RCC panel allows air pressure to equalize behind the RCC panels during ascent and re-entry.

The mid-wing area on the left wing, behind where the breach occurred, is supported by a series of trusses, as shown in red in the figure below. The mid-wing area is bounded in the front and back by the Xo1040 and Xo1191 cross spars, respectively. The numerical designation of each spar comes from its location along the Orbiter's X-axis; for example, the Xo1040 spar is 1,040 inches from the zero point on the X-axis. The cross spars provide the wing's structural integrity. Three major cross spars behind the Xo1191 spar provide the primary structural strength for the aft portion of the wing. The inboard portion of the mid-wing is the outer wall of the left wheel-well, and the outboard portion of the mid-wing is the wing leading edge spar, where the RCC panels attach.



The Wing Leading Edge Structural System on Columbia.



The major internal support structures in the mid-wing are constructed from aluminum alloy. Since aluminum melts at 1,200 degrees Fahrenheit, it is likely these truss tubes in the mid-wing were destroyed and wing structural integrity was lost.

fallout rate was generally less than previously recorded except for one location, which had the highest rate of zinc fallout of all the samples from both evaluations. Chemical analysis of the most recent rainwater samples determined the percentage of zinc to be consistently around nine percent, with that one exception.

Specimens with pinholes were fabricated from RCC panel 12-right and arc-jet-tested, but the arc-jet testing did not substantially change the pinhole dimensions or substrate oxidation. (Arc jet testing is done in a wind tunnel with an electrical arc that provides an airflow of up to 2,800 degrees Fahrenheit.) As a result of the pinhole investigation, the sealant refurbishment process was revised to include cleaning the part in a vacuum at 2,000 degrees Fahrenheit to bake out contaminants like zinc oxide and salt, and forcing sealant into pinholes.

Post-flight analysis of RCC components confirms that sealant is ablated during each mission, which increases subsurface oxidation and reduces component strength and mission life. Based on the destructive evaluation of *Columbia's* panel 12-right and various arc-jet tests, refurbishment intervals were established to achieve the desired service life.

In November 2001, white residue was discovered on about half the RCC panels on *Columbia*, *Atlantis*, and *Endeavour*. Investigations revealed that the deposits were sodium carbonate that resulted from the exposure of sealant to rainwater, with three possible outcomes: (1) the deposits are washed off, which decreases sealant effectiveness; (2) the deposits remain on the part's surface, melt on re-entry, and combine with the glass, restoring the sealant composition; or (3) the deposits remain on the part's surface, melt on re-entry, and flow onto metal parts.

The root cause of the white deposits on the surface of RCC parts was the breakdown of the sealant. This does not damage RCC material.

### Non-Destructive Evaluations of Reinforced Carbon-Carbon Components

Over the 20 years of Space Shuttle operations, RCC has performed extremely well in the harsh environment it is exposed to during a mission. Within the last several years, a few instances of damage to RCC material have resulted in a re-examination of the current visual inspection process. Concerns about potential oxidation between the silicon carbide layer and the substrate and within the substrate has resulted in further efforts to develop improved Non-Destructive Evaluation methods and a better understanding of subsurface oxidation.

Since 1997, inspections have revealed five instances of RCC silicon carbide layer loss with exposed substrate. In November 1997, *Columbia* returned from STS-87 with three damaged RCC parts with carbon substrate exposed. Panel 19-right had a 0.04 inch-diameter by 0.035 inch-deep circular dimple, panel 17-right had a 0.1 inch-wide by 0.2 inch-long by 0.025-inch-deep dimple, and the Orbiter forward External Tank attachment point had a 0.2-inch by 0.15-inch

by 0.026-inch-deep dimple. In January 2000, after STS-103, *Discovery's* panel 8-left was scrapped because of similar damage (see Figure 3.3-5).

In April 2001, after STS-102, *Columbia's* panel 10-left had a 0.2-inch by 0.3-inch wide by 0.018-inch-deep dimple in the panel corner next to the T-seal. The dimple was repaired and the panel flew one more mission, then was scrapped because of damage found in the repair.

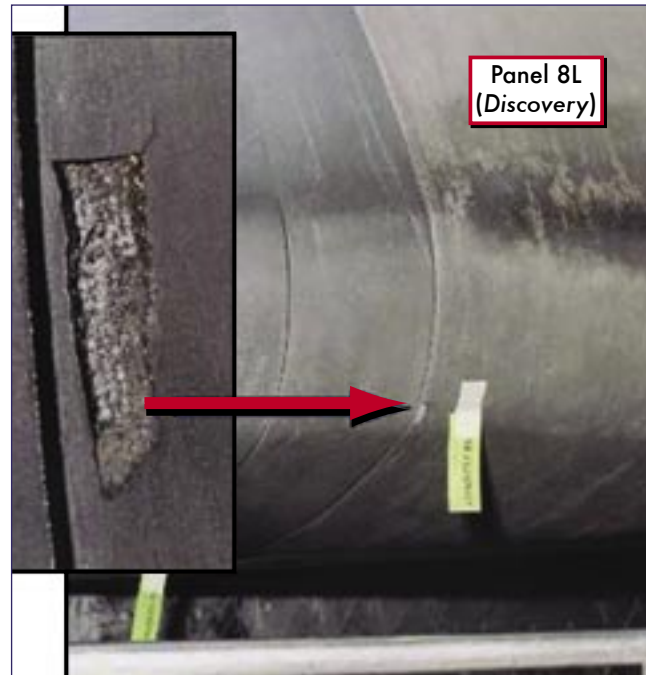


Figure 3.3-5. RCC panel 8-left from *Discovery* had to be scrapped after STS-103 because of the damage shown here.

### Findings:

- F3.3-1 The original design specifications required the RCC components to have essentially no impact resistance.
- F3.3-2 Current inspection techniques are not adequate to assess structural integrity of the RCC components.
- F3.3-3 After manufacturer's acceptance non-destructive evaluation, only periodic visual and touch tests are conducted.
- F3.3-4 RCC components are weakened by mass loss caused by oxidation within the substrate, which accumulates with age. The extent of oxidation is not directly measurable, and the resulting mission life reduction is developed analytically.
- F3.3-5 To date, only two flown RCC panels, having achieved 15 and 19 missions, have been destructively tested to determine actual loss of strength due to oxidation.
- F3.3-6 Contamination from zinc leaching from a primer under the paint topcoat on the launch pad structure increases the opportunities for localized oxidation.

**Recommendations:**

- R3.3-1 Develop and implement a comprehensive inspection plan to determine the structural integrity of all Reinforced Carbon-Carbon system components. This inspection plan should take advantage of advanced non-destructive inspection technology.
- R3.3-2 Initiate a program designed to increase the Orbiter's ability to sustain minor debris damage by measures such as improved impact-resistant Reinforced Carbon-Carbon and acreage tiles. This program should determine the actual impact resistance of current materials and the effect of likely debris strikes.
- R3.3-3 To the extent possible, increase the Orbiter's ability to successfully re-enter the Earth's atmosphere with minor leading edge structural sub-system damage.
- R3.3-4 In order to understand the true material characteristics of Reinforced Carbon-Carbon components, develop a comprehensive database of flown Reinforced Carbon-Carbon material characteristics by destructive testing and evaluation.
- R3.3-5 Improve the maintenance of launch pad structures to minimize the leaching of zinc primer onto Reinforced Carbon-Carbon components.

**3.4 IMAGE AND TRANSPORT ANALYSES**

At 81.9 seconds after launch of STS-107, a sizable piece of foam struck the leading edge of *Columbia's* left wing. Visual evidence established the source of the foam as the left bipod ramp area of the External Tank. The widely accepted implausibility of foam causing significant damage to the wing leading edge system led the Board to conduct independent tests to characterize the impact. While it was impossible to determine the precise impact parameters because of uncertainties about the foam's density, dimensions, shape, and initial velocity, intensive work by the Board, NASA, and contractors provided credible ranges for these elements. The

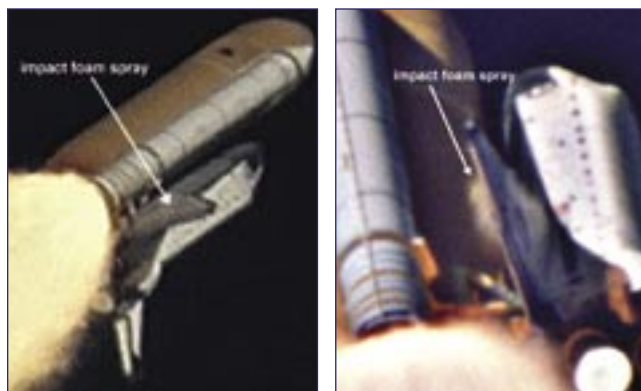


Figure 3.4-1 (color enhanced and "de-blurred" by Lockheed Martin Gaithersburg) and Figure 3.4-2 (processed by the National Imagery and Mapping Agency) are samples of the type of visual data used to establish the time of the impact (81.9 seconds), the altitude at which it occurred (65,860 feet), and the object's relative velocity at impact (about 545 mph relative to the Orbiter).

Board used a combination of tests and analyses to conclude that the foam strike observed during the flight of STS-107 was the direct, physical cause of the accident.

**Image Analysis: Establishing Size, Velocity, Origin, and Impact Area**

The investigation image analysis team included members from Johnson Space Center Image Analysis, Johnson Space Center Engineering, Kennedy Space Center Photo Analysis, Marshall Space Flight Center Photo Analysis, Lockheed Martin Management and Data Systems, the National Imagery and Mapping Agency, Boeing Systems Integration, and Langley Research Center. Each member of the image analysis team performed independent analyses using tools and methods of their own choosing. Representatives of the Board participated regularly in the meetings and deliberations of the image analysis team.

A 35-mm film camera, E212, which recorded the foam strike from 17 miles away, and video camera E208, which recorded it from 26 miles away, provided the best of the available evidence. Analysis of this visual evidence (see Figures 3.4-1 and 3.4-2) along with computer-aided design analysis, refined the potential impact area to less than 20 square feet in RCC panels 6 through 9 (see Figure 3.4-3), including a portion of the corresponding carrier panels and adjacent tiles. The investigation image analysis team found no conclusive visual evidence of post-impact debris flowing over the top of the wing.

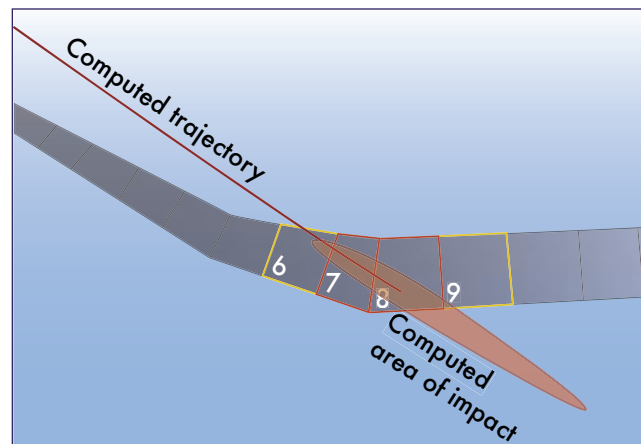
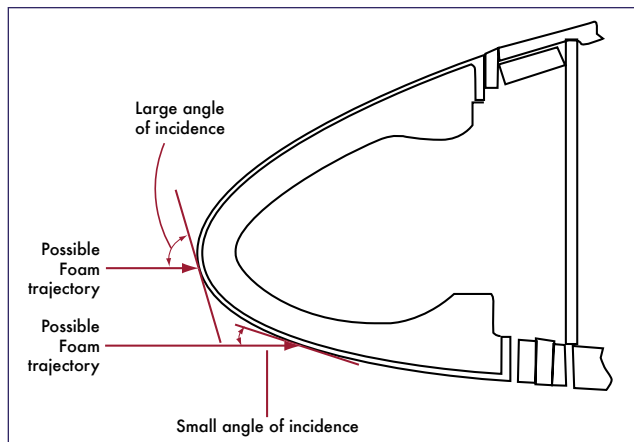


Figure 3.4-3: The best estimate of the site of impact by the center of the foam.

The image analysis team established impact velocities from 625 to 840 feet per second (about 400 to 600 mph) relative to the Orbiter, and foam dimensions from 21 to 27 inches long by 12 to 18 inches wide.<sup>8</sup> The wide range for these measurements is due primarily to the cameras' relatively slow frame rate and poor resolution. For example, a 20-inch change in the position of the foam near the impact point would change the estimated relative impact speed from 675 feet per second to 825 feet per second. The visual evidence could not reveal the foam's shape, but the team was able to describe it as flat and relatively thin. The mass and hence the volume of the

foam was determined from the velocity estimates and their ballistic coefficients.

Image analysis determined that the foam was moving almost parallel to the Orbiter's fuselage at impact, with about a five-degree angle upward toward the bottom of the wing and slight motion in the outboard direction. If the foam had hit the tiles adjacent to the leading edge, the angle of incidence would have been about five degrees (the angle of incidence is the angle between the relative velocity of the projectile and the plane of the impacted surface). Because the wing leading edge curves, the angle of incidence increases as the point of impact approaches the apex of an RCC panel. Image and transport analyses estimated that for impact on RCC panel 8, the angle of incidence was between 10 and 20 degrees (see Figure 3.4-4).<sup>9</sup> Because the total force delivered by the impact depends on the angle of incidence, a foam strike near the apex of an RCC panel could have delivered about twice the force as an impact close to the base of the panel.



*Figure 3.4-4. This drawing shows the curve of the wing leading edge and illustrates the difference the angle of incidence has on the effect of the foam strike.*

Despite the uncertainties and potential errors in the data, the Board concurred with conclusions made unanimously by the post-flight image analysis team and concludes the information available about the foam impact during the mission was adequate to determine its effect on both the thermal tiles and RCC. Those conclusions made during the mission follow:

- The bipod ramp was the source of the foam.
- Multiple pieces of foam were generated, but there was no evidence of more than one strike to the Orbiter.
- The center of the foam struck the leading edge structural subsystem of the left wing between panels 6 to 9. The potential impact location included the corresponding carrier panels, T-seals, and adjacent tiles. (Based on further image analysis performed by the National Imagery and Mapping Agency, the transport analysis that follows, and forensic evidence, the Board concluded that a smaller estimated impact area in the immediate vicinity of panel 8 was credible.)
- Estimates of the impact location and velocities rely on timing of camera images and foam position measurements.
- The relative velocity of the foam at impact was 625 to 840 feet per second. (The Board agreed on a narrower speed range based on a transport analysis that follows.)
- The trajectory of the foam at impact was essentially parallel to the Orbiter's fuselage.
- The foam was making about 18 revolutions per second as it fell.
- The orientation at impact could not be determined.
- The foam that struck the wing was 24 (plus or minus 3) inches by 15 (plus or minus 3) inches. The foam shape could only be described as flat. (A subsequent transport analysis estimated a thickness.)
- Ice was not present on the external surface of the bipod ramp during the last Ice Team camera scan prior to launch (at approximately T-5 minutes).
- There was no visual evidence of the presence of other materials inside the bipod ramp.
- The foam impact generated a cloud of pulverized debris with very little component of velocity away from the wing.

- In addition, the visual evidence showed two sizable, traceable post-strike debris pieces with a significant component of velocity away from the wing.

Although the investigation image analysis team found no evidence of post-strike debris going over the top of the wing before or after impact, a colorimetric analysis by the National Imagery and Mapping Agency indicated the potential presence of debris material over the top of the left wing immediately following the foam strike. This analysis suggests that some of the foam may have struck closer to the apex of the wing than what occurred during the impact tests described below.

### Imaging Issues

The image analysis was hampered by the lack of high resolution and high speed ground-based cameras. The existing camera locations are a legacy of earlier NASA programs, and are not optimum for the high-inclination Space Shuttle missions to the International Space Station and oftentimes

## THE ORBITER "RAN INTO" THE FOAM

"How could a lightweight piece of foam travel so fast and hit the wing at 545 miles per hour?"

Just prior to separating from the External Tank, the foam was traveling with the Shuttle stack at about 1,568 mph (2,300 feet per second). Visual evidence shows that the foam debris impacted the wing approximately 0.161 seconds after separating from the External Tank. In that time, the velocity of the foam debris slowed from 1,568 mph to about 1,022 mph (1,500 feet per second). Therefore, the Orbiter hit the foam with a relative velocity of about 545 mph (800 feet per second). In essence, the foam debris slowed down and the Orbiter did not, so the Orbiter ran into the foam. The foam slowed down rapidly because such low-density objects have low ballistic coefficients, which means their speed rapidly decreases when they lose their means of propulsion.

	<i>Minimum Impact Speed (mph)</i>	<i>Maximum Impact Speed (mph)</i>	<i>Best Estimated Impact Speed (mph)</i>	<i>Minimum Volume (cubic inches)</i>	<i>Maximum Volume (cubic inches)</i>	<i>Best Estimated Volume (cubic inches)</i>
During STS-107	375	654	477	400	1,920	1,200
After STS-107	528	559	528	1,026	1,239	1,200

Figure 3.4-5. The best estimates of velocities and volumes calculated during the mission and after the accident based on visual evidence and computer analyses. Information available during the mission was adequate to determine the foam's effect on both thermal tiles and RCC.

cameras are not operating or, as in the case of STS-107, out of focus. Launch Commit Criteria should include that sufficient cameras are operating to track the Shuttle from liftoff to Solid Rocket Booster separation.

Similarly, a developmental vehicle like the Shuttle should be equipped with high resolution cameras that monitor potential hazard areas. The wing leading edge system, the area around the landing gear doors, and other critical Thermal Protection System elements need to be imaged to check for damage. Debris sources, such as the External Tank, also need to be monitored. Such critical images need to be downlinked so that potential problems are identified as soon as possible.

### Transport Analysis: Establishing Foam Path by Computational Fluid Dynamics

Transport analysis is the process of determining the path of the foam. To refine the Board's understanding of the foam strike, a transport analysis team, consisting of members from Johnson Space Center, Ames Research Center, and Boeing, augmented the image analysis team's research.

A variety of computer models were used to estimate the volume of the foam, as well as to refine the estimates of its velocity, its other dimensions, and the impact location. Figure 3.4-5 lists the velocity and foam size estimates produced during the mission and at the conclusion of the investigation.

The results listed in Figure 3.4-5 demonstrate that reasonably accurate estimates of the foam size and impact velocity were available during the mission. Despite the lack of high-quality visual evidence, the input data available to assess the impact damage during the mission was adequate.

The input data to the transport analysis consisted of the computed airflow around the Shuttle stack when the foam was shed, the estimated aerodynamic characteristics of the foam, the image analysis team's trajectory estimates, and the size and shape of the bipod ramp.

The transport analysis team screened several of the image analysis team's location estimates, based on the feasible aerodynamic characteristics of the foam and the laws of physics. Optical distortions caused by the atmospheric density gradients associated with the shock waves off the Orbiter's nose, External Tank, and Solid Rocket Boosters may have compromised the image analysis team's three position estimates closest to the bipod ramp. In addition, the image analysis team's position estimates closest to the wing were compromised by the lack of two camera views and the shock

region ahead of the wing, making triangulation impossible and requiring extrapolation. However, the transport analysis confirmed that the image analysis team's estimates for the central portion of the foam trajectory were well within the computed flow field and the estimated range of aerodynamic characteristics of the foam.

The team identified a relatively narrow range of foam impact velocities and ballistic coefficients. The ballistic coefficient of an object expresses the relative influence of weight and atmospheric drag on it, and is the primary aerodynamic characteristic of an object that does not produce lift. An object with a large ballistic coefficient, such as a cannon ball, has a trajectory that can be computed fairly accurately without accounting for drag. In contrast, the foam that struck the wing had a relatively small ballistic coefficient with a large drag force relative to its weight, which explains why it slowed down quickly after separating from the External Tank. Just prior to separation, the speed of the foam was equal to the speed of the Shuttle, about 1,568 mph (2,300 feet per second). Because of a large drag force, the foam slowed to about 1,022 mph (1,500 feet per second) in about 0.2 seconds, and the Shuttle struck the foam at a relative

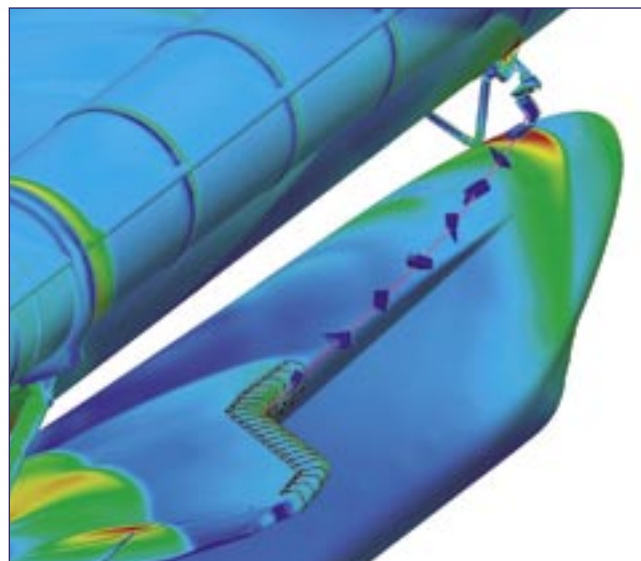


Figure 3.4-6. These are the results of a trajectory analysis that used a computational fluid dynamics approach in a program called CART-3D, a comprehensive (six-degree-of-freedom) computer simulation based on the laws of physics. This analysis used the aerodynamic and mass properties of bipod ramp foam, coupled with the complex flow field during ascent, to determine the likely position and velocity histories of the foam.

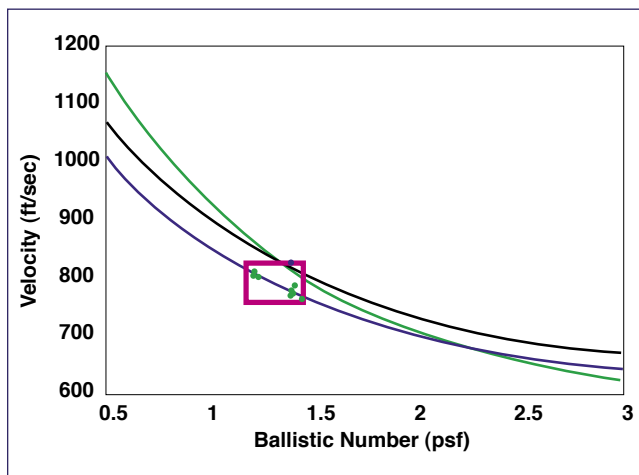


Figure 3.4-7. The results of numerous possible trajectories based on various assumed sizes, shapes, and densities of the foam. Either the foam had a slightly higher ballistic coefficient and the Orbiter struck the foam at a lower speed relative to the Orbiter, or the foam was more compact and the wing struck the foam at a higher speed. The “best fit” box represents the overlay of the data from the image analysis with the transport analysis computations. This data enabled a final selection of projectile characteristics for impact testing.

speed of about 545 mph (800 feet per second). (See Appendix D.8.)

The undetermined and yet certainly irregular shape of the foam introduced substantial uncertainty about its estimated aerodynamic characteristics. Appendix D.8 contains an independent analysis conducted by the Board to confirm that the estimated range of ballistic coefficients of the foam in Figure 3.4-6 was credible, given the foam dimension results from the image analyses and the expected range of the foam density. Based on the results in Figure 3.4-7, the physical dimensions of the bipod ramp, and the sizes and shapes of the available barrels for the compressed-gas gun used in the impact test program described later in this chapter, the Board and the NASA Accident Investigation Team decided that a foam projectile 19 inches by 11.5 inches by 5.5 inches, weighing 1.67 pounds, and with a weight density of 2.4 pounds per cubic foot, would best represent the piece of foam that separated from the External Tank bipod ramp and was hit by the Orbiter’s left wing. See Section 3.8 for a full discussion of the foam impact testing.

**Findings:**

- F3.4-1 Photographic evidence during ascent indicates the projectile that struck the Orbiter was the left bipod ramp foam.
- F3.4-2 The same photographic evidence, confirmed by independent analysis, indicates the projectile struck the underside of the leading edge of the left wing in the vicinity of RCC panels 6 through 9 or the tiles directly behind, with a velocity of approximately 775 feet per second.
- F3.4-3 There is a requirement to obtain and downlink

on-board engineering quality imaging from the Shuttle during launch and ascent.

- F3.4-4 The current long-range camera assets on the Kennedy Space Center and Eastern Range do not provide best possible engineering data during Space Shuttle ascents.
- F3.4-5 Evaluation of STS-107 debris impact was hampered by lack of high resolution, high speed cameras (temporal and spatial imagery data).
- F3.4-6 Despite the lack of high quality visual evidence, the information available about the foam impact during the mission was adequate to determine its effect on both the thermal tiles and RCC.

**Recommendations:**

- R3.4-1 Upgrade the imaging system to be capable of providing a minimum of three useful views of the Space Shuttle from liftoff to at least Solid Rocket Booster separation, along any expected ascent azimuth. The operational status of these assets should be included in the Launch Commit Criteria for future launches. Consider using ships or aircraft to provide additional views of the Shuttle during ascent.
- R3.4-2 Provide a capability to obtain and downlink high-resolution images of the External Tank after it separates.
- R3.4-3 Provide a capability to obtain and downlink high-resolution images of the underside of the Orbiter wing leading edge and forward section of both wings’ Thermal Protection System.

**3.5 ON-ORBIT DEBRIS SEPARATION – THE “FLIGHT DAY 2” OBJECT**

Immediately after the accident, Air Force Space Command began an in-depth review of its Space Surveillance Network data to determine if there were any detectable anomalies during the STS-107 mission. A review of the data resulted in no information regarding damage to the Orbiter. However, Air Force processing of Space Surveillance Network data yielded 3,180 separate radar or optical observations of the Orbiter from radar sites at Eglin, Beale, and Kirtland Air Force Bases, Cape Cod Air Force Station, the Air Force Space Command’s Maui Space Surveillance System in Hawaii, and the Navy Space Surveillance System. These observations, examined after the accident, showed a small object in orbit with *Columbia*. In accordance with the International Designator system, the object was named 2003-003B (*Columbia* was designated 2003-003A). The timeline of significant events includes:

1. January 17, 2003, 9:42 a.m. Eastern Standard Time: Orbiter moves from tail-first to right-wing-first orientation
2. January 17, 10:17 a.m.: Orbiter returns to tail-first orientation
3. January 17, 3:57 p.m.: First confirmed sensor track of object 2003-003B
4. January 17, 4:46 p.m.: Last confirmed sensor track for this date

5. January 18: Object reacquired and tracked by Cape Cod Air Force Station PAVE PAWS
6. January 19: Object reacquired and tracked by Space Surveillance Network
7. January 20, 8:45 – 11:45 p.m.: 2003-003B orbit decays. Last track by Navy Space Surveillance System

Events around the estimated separation time of the object were reviewed in great detail. Extensive on-board sensor data indicates that no unusual crew activities, telemetry data, or accelerations in Orbiter or payload can account for the release of an object. No external mechanical systems were active, nor were any translational (forward, backward, or sideways, as opposed to rotational) maneuvers attempted in this period. However, two attitude maneuvers were made: a 48-degree yaw maneuver to a left-wing-forward and payload-bay-to-Earth attitude from 9:42 to 9:46 a.m. EST), and

a maneuver back to the bay-to-Earth, tail-forward attitude from 10:17 to 10:21 a.m. It is possible that this maneuver imparted the initial departure velocity to the object.

Although various Space Surveillance Network radars tracked the object, the only reliable physical information includes the object's ballistic coefficient in kilograms per square meter and its radar cross-section in decibels per square meter. An object's radar cross-section relates how much radar energy the object scatters. Since radar cross-section depends on the object's material properties, shape, and orientation relative to the radar, the Space Surveillance Network could not independently estimate the object's size or shape. By radar observation, the object's Ultra-High Frequency (UHF) radar cross-section varied between 0.0 and minus 18.0 decibels per square meter (plus or minus 1.3 decibels), and its ballistic coefficient was known to be 0.1 kilogram per meter squared (plus or minus 15 percent). These two quantities were used to test and ultimately eliminate various objects.

### ON-ORBIT COLLISION AVOIDANCE

The Space Control Center, operated by the 21st Space Wing's 1st Space Control Squadron (a unit of Air Force Space Command), maintains an orbital data catalog on some 9,000 Earth-orbiting objects, from active satellites to space debris, some of which may be as small as four inches. The Space Control Center ensures that no known orbiting objects will transit an Orbiter "safety zone" measuring 6 miles deep by 25 miles wide and long (Figure A) during a Shuttle mission by projecting the Orbiter's flight path for the next 72 hours (Figure B) and comparing it to the flight paths of all known orbiting or re-entering objects, which generally travel at 17,500 miles per hour. Whenever possible, the Orbiter moves tail-first while on orbit to minimize the chances of orbital debris or micrometeoroids impacting the cabin windscreen or the Orbiter's wing leading edge.

If an object is determined to be within 36-72 hours of colliding with the Orbiter, the Space Control Center notifies NASA, and the agency then determines a maneuver to avoid a collision. There were no close approaches to *Columbia* detected during STS-107.

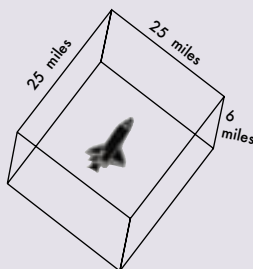


Figure A. Orbiter Safety Zone

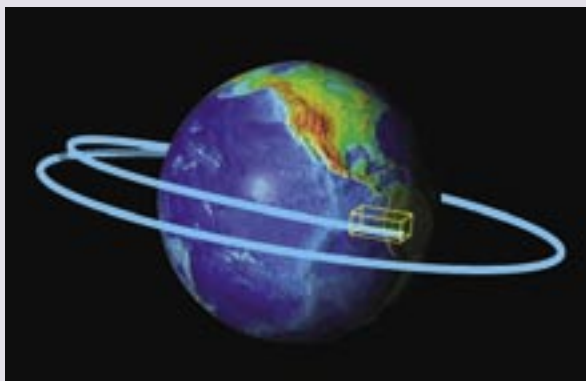


Figure B. Protecting the Orbiter's flight path

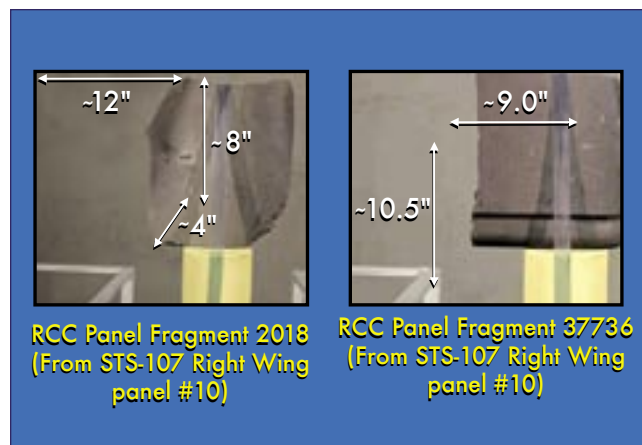


Figure 3.5-1. These representative RCC acreage pieces matched the radar cross-section of the Flight Day 2 object.

In the Advanced Compact Range at the Air Force Research Laboratory in Dayton, Ohio, analysts tested 31 materials from the Orbiter's exterior and payload bay. Additional supercomputer radar cross-section predictions were made for Reinforced Carbon-Carbon T-seals. After exhaustive radar cross-section analysis and testing, coupled with ballistic analysis of the object's orbital decay, only a fragment of RCC panel would match the UHF radar cross-section and ballistic coefficients observed by the Space Surveillance network. Such an RCC panel fragment must be approximately 140 square inches or greater in area to meet the observed radar cross-section characteristics. Figure 3.5-1 shows RCC panel fragments from *Columbia*'s right wing that represent those meeting the observed characteristics of object 2003-003B.<sup>10</sup>

Note that the Southwest Research Institute foam impact test on panel 8 (see Section 3.8) created RCC fragments that fell into the wing cavity. These pieces are consistent in size with the RCC panel fragments that exhibited the required physical characteristics consistent with the Flight Day 2 object.

## Findings:

- F3.5-1 The object seen on orbit with *Columbia* on Flight Day 2 through 4 matches the radar cross-section and area-to-mass measurements of an RCC panel fragment.
- F3.5-2 Though the Board could not positively identify the Flight Day 2 object, the U.S. Air Force exclusionary test and analysis processes reduced the potential Flight Day 2 candidates to an RCC panel fragment.

## Recommendations:

- None

## 3.6 DE-ORBIT/RE-ENTRY

As *Columbia* re-entered Earth's atmosphere, sensors in the Orbiter relayed streams of data both to entry controllers on the ground at Johnson Space Center and to the Modular Auxiliary Data System recorder, which survived the breakup of the Orbiter and was recovered by ground search teams. This data – temperatures, pressures, and stresses – came from sensors located throughout the Orbiter. Entry controllers were unaware of any problems with re-entry until telemetry data indicated errant readings. During the investigation data from these two sources was used to make aerodynamic, aerothermal, and mechanical reconstructions of re-entry that showed how these stresses affected the Orbiter.

The re-entry analysis and testing focused on eight areas:

1. Analysis of the Modular Auxiliary Data System recorder information and the pattern of wire runs and sensor failures throughout the Orbiter.
2. Physical and chemical analysis of the recovered debris to determine where the breach in the RCC panels likely occurred.
3. Analysis of videos and photography provided by the general public.
4. Abnormal heating on the outside of the Orbiter body. Sensors showed lower heating and then higher heating than is usually seen on the left Orbital Maneuvering System pod and the left side of the fuselage.
5. Early heating inside the wing leading edge. Initially, heating occurred inside the left wing RCC panels before the wing leading edge spar was breached.
6. Later heating inside the left wing structure. This analysis focused on the inside of the left wing after the wing leading edge spar had been breached.
7. Early changes in aerodynamic performance. The Orbiter began reacting to increasing left yaw and left roll, consistent with developing drag and loss of lift on the left wing.
8. Later changes in aerodynamic performance. Almost 600 seconds after Entry Interface, the left-rolling tendency of the Orbiter changes to a right roll, indicating an increase in lift on the left wing. The left yaw also increased, showing increasing drag on the left wing.

For a complete compilation of all re-entry data, see the

CAIB/NAIT Working Scenario (Appendix D.7) and the Re-entry Timeline (Appendix D.9). The extensive aerothermal calculations and wind tunnel tests performed to investigate the observed re-entry phenomenon are documented in NASA report NSTS-37398.

## Re-Entry Environment

In the demanding environment of re-entry, the Orbiter must withstand the high temperatures generated by its movement through the increasingly dense atmosphere as it decelerates from orbital speeds to land safely. At these velocities, shock waves form at the nose and along the leading edges of the wing, intersecting near RCC panel 9. The interaction between these two shock waves generates extremely high temperatures, especially around RCC panel 9, which experiences the highest surface temperatures of all the RCC panels. The flow behind these shock waves is at such a high temperature that air molecules are torn apart, or “dissociated.” The air immediately around the leading edge surface can reach 10,000 degrees Fahrenheit; however, the boundary layer shields the Orbiter so that the actual temperature is only approximately 3,000 degrees Fahrenheit at the leading edge. The RCC panels and internal insulation protect the aluminum wing leading edge spar. A breach in one of the leading-edge RCC panels would expose the internal wing structure to temperatures well above 3,000 degrees Fahrenheit.

In contrast to the aerothermal environment, the aerodynamic environment during *Columbia*'s re-entry was relatively benign, especially early in re-entry. The re-entry dynamic pressure ranged from zero at Entry Interface to 80 pounds per square foot when the Orbiter went out of control, compared with a dynamic pressure during launch and ascent of nearly 700 pounds per square foot. However, the aerodynamic forces were increasing quickly during the final minutes of *Columbia*'s flight, and played an important role in the loss of control.

## Orbiter Sensors

The Operational Flight Instrumentation monitors physical sensors and logic signals that report the status of various Orbiter functions. These sensor readings and signals are telemetered via a 128 kilobit-per-second data stream to the Mission Control Center, where engineers ascertain the real-time health of key Orbiter systems. An extensive review of this data has been key to understanding what happened to STS-107 during ascent, orbit, and re-entry.

The Modular Auxiliary Data System is a supplemental instrumentation system that gathers Orbiter data for processing after the mission is completed. Inputs are almost exclusively physical sensor readings of temperatures, pressures, mechanical strains, accelerations, and vibrations. The Modular Auxiliary Data System usually records only the mission's first and last two hours (see Figure 3.6-1).

The Orbiter Experiment instrumentation is an expanded suite of sensors for the Modular Auxiliary Data System that was installed on *Columbia* for engineering development purposes. Because *Columbia* was the first Orbiter launched,



Figure 3.6-1. The Modular Auxiliary Data System recorder, found near Hemphill, Texas. While not designed to withstand impact damage, the recorder was in near-perfect condition when recovered on March 19, 2003.

engineering teams needed a means to gather more detailed flight data to validate their calculations of conditions the vehicle would experience during critical flight phases. The instrumentation remained on *Columbia* as a legacy of the development process, and was still providing valuable flight data from ascent, de-orbit, and re-entry for ongoing flight analysis and vehicle engineering. Nearly all of *Columbia*'s sensors were specified to have only a 10-year shelf life, and in some cases an even shorter service life.

At 22 years old, the majority of the Orbiter Experiment instrumentation had been in service twice as long as its specified service life, and in fact, many sensors were already failing. Engineers planned to stop collecting and analyzing data once most of the sensors had failed, so failed sensors and wiring were not repaired. For instance, of the 181 sensors in *Columbia*'s wings, 55 had already failed or were producing questionable readings before STS-107 was launched.

### Re-Entry Timeline

Times in the following section are noted in seconds elapsed from the time *Columbia* crossed Entry Interface (EI) over the Pacific Ocean at 8:44:09 a.m. EST. *Columbia*'s destruction occurred in the period from Entry Interface at 400,000 feet (EI+000) to about 200,000 feet (EI+970) over Texas. The Modular Auxiliary Data System recorded the first indications of problems at EI plus 270 seconds (EI+270). Because data from this system is retained onboard, Mission Control did not notice any troubling indications from telemetry data until 8:54:24 a.m. (EI+613), some 10 minutes after Entry Interface.

### Left Wing Leading Edge Spar Breach (EI+270 through EI+515)

At EI+270, the Modular Auxiliary Data System recorded the first unusual condition while the Orbiter was still over the Pacific Ocean. Four sensors, which were all either inside

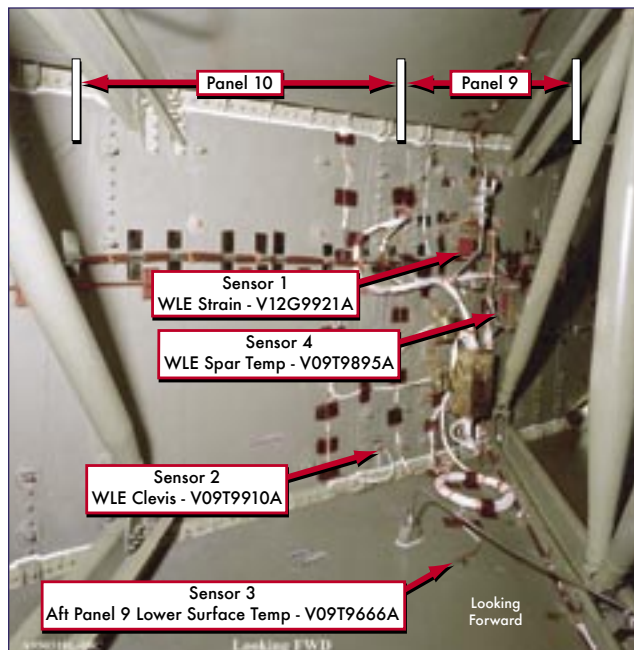


Figure 3.6-2. Location of sensors on the back of the left wing leading edge spar (vertical aluminum structure in picture). Also shown are the round truss tubes and ribs that provided the structural support for the mid-wing in this area.

or outside the wing leading edge spar near Reinforced Carbon-Carbon (RCC) panel 9-left, helped tell the story of what happened on the left wing of the Orbiter early in the re-entry. These four sensors were: strain gauge V12G9921A (Sensor 1), resistance temperature detector V09T9910A on the RCC clevis between panel 9 and 10 (Sensor 2), thermocouple V07T9666A, within a Thermal Protection System tile (Sensor 3), and resistance temperature detector V09T9895A (Sensor 4), located on the back side of the wing leading edge spar behind RCC panels 8 and 9 (see Figure 3.6-2).

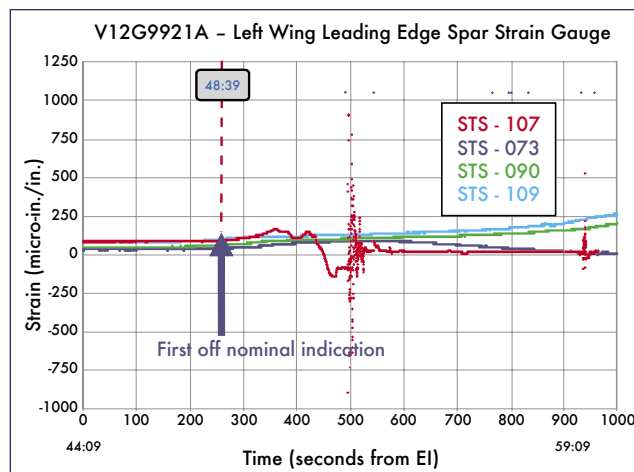


Figure 3.6-3. The strain gauge (Sensor 1) on the back of the left wing leading edge spar was the first sensor to show an anomalous reading. In this chart, and the others that follow, the red line indicates data from STS-107. Data from other *Columbia* re-entries, similar to the STS-107 re-entry profile, are shown in the other colors.

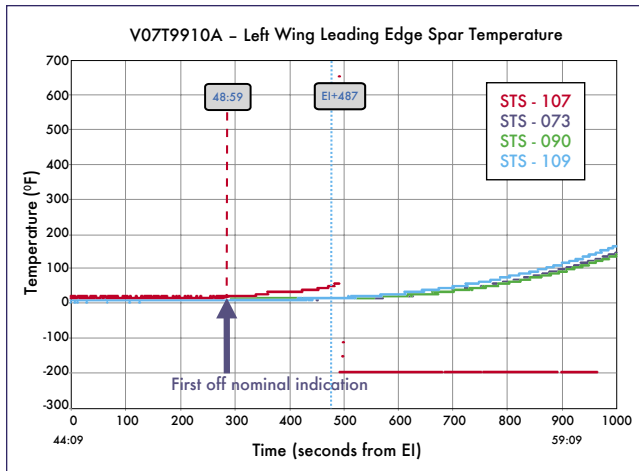


Figure 3.6-4. This temperature thermocouple (Sensor 2) was mounted on the outside of the wing leading edge spar behind the insulation that protects the spar from radiated heat from the RCC panels. It clearly showed an off-nominal trend early in the re-entry sequence and began to show an increase in temperature much earlier than the temperature sensor behind the spar.

Sensor 1 provided the first anomalous reading (see Figure 3.6-3). From EI+270 to EI+360, the strain is higher than that on previous *Columbia* flights. At EI+450, the strain reverses, and then peaks again in a negative direction at EI+475. The strain then drops slightly, and remains constant and negative until EI+495, when the sensor pattern becomes unreliable, probably due to a propagating soft short, or “burn-through” of the insulation between cable conductors caused by heating or combustion. This strain likely indicates significant damage to the aluminum honeycomb spar. In particular, strain reversals, which are unusual, likely mean there was significant high-temperature damage to the spar during this time.

At EI+290, 20 seconds after Sensor 1 gave its first anomalous reading, Sensor 2, the only sensor in the front of the

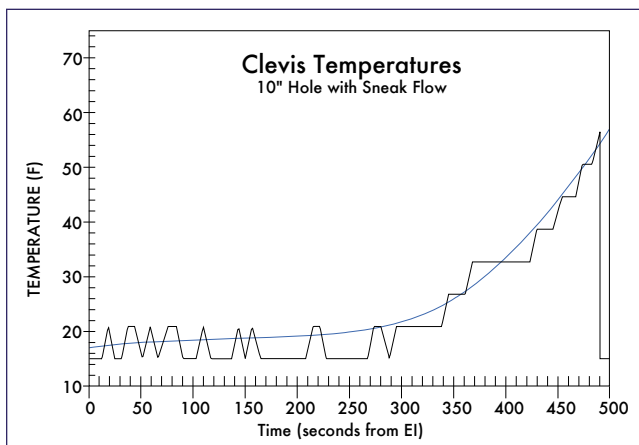


Figure 3.6-5. The analysis of the effect of a 10-inch hole in RCC panel 8 on Sensor 2 from EI to EI+500 seconds. The jagged line shows the actual flight data readings and the smooth line the calculated result for a 10-inch hole with some sneak flow of superheated air behind the spar insulation.

left wing leading edge spar, recorded the beginning of a gradual and abnormal rise in temperature from an expected 30 degrees Fahrenheit to 65 degrees at EI+493, when it then dropped to “off-scale low,” a reading that drops off the scale at the low end of the sensor’s range (see Figure 3.6-4). Sensor 2, one of the first to fail, did so abruptly. It had indicated only a mild warming of the RCC attachment clevis before the signal was lost.

A series of thermal analyses were performed for different sized holes in RCC panel 8 to compute the time required to heat Sensor 2 to the temperature recorded by the Modular Auxiliary Data System. To heat the clevis, various insulators would have to be bypassed with a small amount of leakage, or “sneak flow.” Figure 3.6-5 shows the results of these calculations for, as an example, a 10-inch hole, and demonstrates that with sneak flow around the insulation, the temperature profile of the clevis sensor was closely matched by the engineering calculations. This is consistent with the same sneak flow required to match a similar but abnormal ascent temperature rise of the same sensor, which further supports the premise that the breach in the leading edge of the wing occurred during ascent. While the exact size of the breach will never be known, and may have been smaller or larger than 10 inches, these analyses do provide a plausible explanation for the observed rises in temperature sensor data during re-entry.

Investigators initially theorized that the foam might have broken a T-seal and allowed superheated air to enter the wing between the RCC panels. However, the amount of T-seal debris from this area and subsequent aerothermal analysis showing this type of breach did not match the observed damage to the wing, led investigators to eliminate a missing T-seal as the source of the breach.

Although abnormal, the re-entry temperature rise was slow and small compared to what would be expected if Sensor 2 were exposed to a blast of superheated air from an assumed breach in the RCC panels. The slow temperature rise is at-

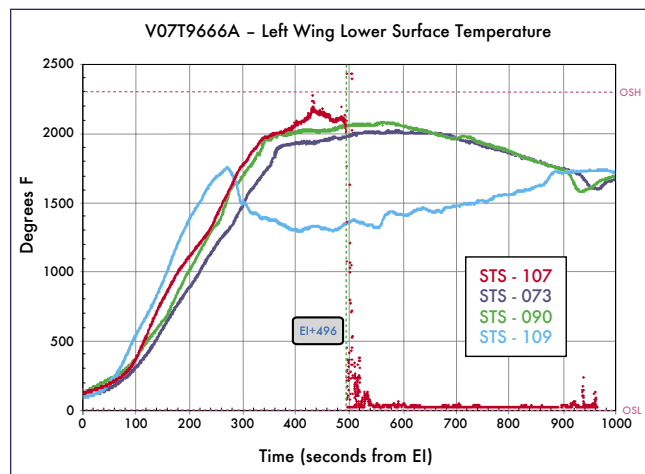


Figure 3.6-6. As early as EI+370, Sensor 3 began reading significantly higher than on previous flights. Since this sensor was located in a thermal tile on the lower surface of the left wing, its temperatures are much higher than those for the other sensors.

tributed to the presence of a relatively modest breach in the RCC, the thick insulation that surrounds the sensor, and the distance from the site of the breach in RCC panel 8 to the clevis sensor.

The readings of Sensor 3, which was in a thermal tile, began rising abnormally high and somewhat erratically as early as EI+370, with several brief spikes to 2,500 degrees Fahrenheit, significantly higher than the 2,000-degree peak temperature on a normal re-entry (Figure 3.6-6). At EI+496, this reading became unreliable, indicating a failure of the wire or the sensor. Because this thermocouple was on the wing lower surface, directly behind the junction of RCC panel 9 and 10, the high temperatures it initially recorded were almost certainly a result of air jetting through the damaged area of RCC panel 8, or of the normal airflow being disturbed by the damage. Note that Sensor 3 provided an external temperature measurement, while Sensors 2 and 4 provided internal temperature measurements.

Sensor 4 also recorded a rise in temperature that ended in an abrupt fall to off-scale low. Figure 3.6-7 shows that an abnormal temperature rise began at EI+425 and abruptly fell at EI+525. Unlike Sensor 2, this temperature rise was extreme, from an expected 20 degrees Fahrenheit at EI+425 to 40 degrees at EI+485, and then rising much faster to 120 degrees at EI+515, then to an off-scale high (a reading that climbs off the scale at the high end of the range) of 450 degrees at EI+522. The failure pattern of this sensor likely indicates destruction by extreme heat.

The timing of the failures of these four sensors and the path of their cable routing enables a determination of both the timing and location of the breach of the leading edge spar, and indirectly, the breach of the RCC panels. All the cables from these sensors, and many others, were routed into wiring harnesses that ran forward along the back side of the leading edge spar up to a cross spar (see Figure 3.6-8), where they passed through the service opening in the cross spar and then ran in front of the left wheel well before reaching interconnect panel 65P, where they entered the fuselage. All sensors with wiring in this set of harnesses failed between EI+487 to EI+497, except Sensor 4, which survived until EI+522. The diversity of sensor types (temperature, pressure, and strains) and their locations in the left wing indicates that they failed because their wiring was destroyed at spar burn-through, as opposed to destruction of each individual sensor by direct heating.

Examination of wiring installation closeout photographs (pictures that document the state of the area that are normally taken just before access is closed) and engineering drawings show five main wiring harness bundles running forward along the spar, labeled top to bottom as A through E (see Figure 3.6-8). The top four, A through D, are spaced 3 inches apart, while the fifth, E, is 6 inches beneath them. The separation between bundle E and the other four is consistent with the later failure time of Sensor 4 by 25 to 29 seconds, and indicates that the breach was in the upper two-thirds of the spar, causing all but one of the cables in this area to fail between EI+487 to EI+497. The breach then expanded vertically, toward the underside of the wing, causing Sensor 4 to fail 25 seconds

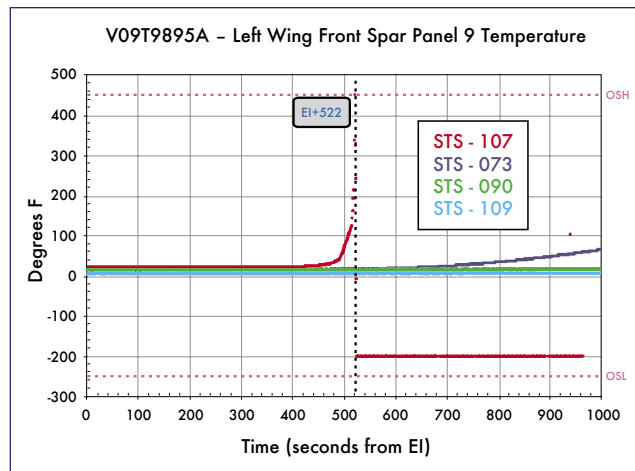


Figure 3.6-7. Sensor 4 also began reading significantly higher than previous flights before it fell off-scale low. The relatively late reaction of this sensor compared to Sensor 2, clearly indicated that superheated air started on the outside of the wing leading edge spar and then moved into the mid-wing after the spar was burned through. Note that immediately before the sensor (or the wire) fails, the temperature is at 450 degrees Fahrenheit and climbing rapidly. It was the only temperature sensor that showed this pattern.

later. Because the distance between bundle A and bundle E is 9 inches, the failure of all these wires indicates that the breach in the wing leading edge spar was at least 9 inches from top to bottom by EI+522 seconds.

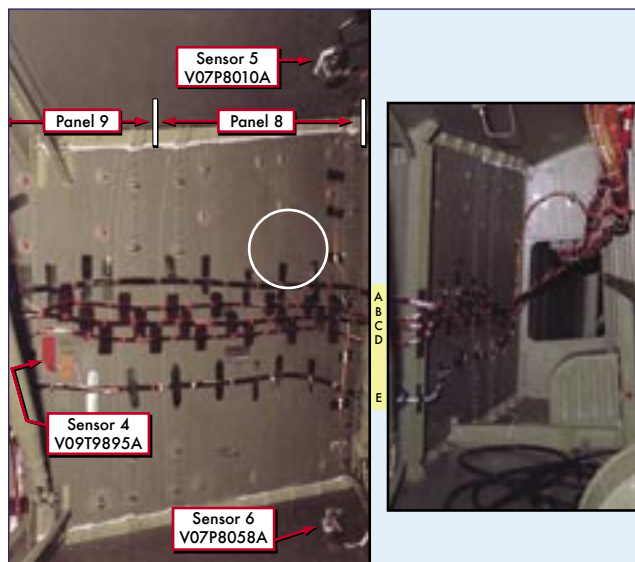


Figure 3.6-8. The left photo above shows the wiring runs on the backside of the wing leading edge behind RCC panel 8 – the circle marks the most likely area where the burn through of the wing leading edge spar initially occurred at EI+487 seconds. The right photo shows the wire bundles as they continue forward behind RCC panels 7 and 6. The major cable bundles in the upper right of the right photo carried the majority of the sensor data inside the wing. As these bundles were burned, controllers on the ground began seeing off-nominal sensor indications.

Also directly behind RCC panel 8 were pressure sensors V07P8010A (Sensor 5), on the upper interior surface of the wing, and V07P8058A (Sensor 6), on the lower interior surface of the wing. Sensor 5 failed abruptly at EI+497. Sensor 6, which was slightly more protected, began failing at EI+495, and failed completely at EI+505. Closeout photographs show that the wiring from Sensor 5 travels down from the top of the wing to join the uppermost harness, A, which then travels along the leading edge spar. Similarly, wiring from Sensor 6 travels up from the bottom of the wing, joins harness A, and continues along the spar. It appears that Sensor 5's wiring, on the upper wing surface, was damaged at EI+497, right after Sensor 1 failed. Noting the times of the sensor failures, and the locations of Sensors 5 and 6 forward of Sensors 1 through 4, spar burn-through must have occurred near where these wires came together.

Two of the 45 left wing strain gauges also recorded an anomaly around EI+500 to EI+580, but their readings were not erratic or off-scale until late in the re-entry, at EI+930. Strain gauge V12G9048A was far forward on a cross spar in the front of the wheel well on the lower spar cap, and strain gauge V12G9049A was on the upper spar cap. Their responses appear to be the actual strain at that location until their failure at EI+935. The exposed wiring for most of the left wing sensors runs along the front of the spar that crosses in front of the left wheel well. The very late failure times of these two sensors indicate that the damage did not spread into the wing cavity forward of the wheel well until at least EI+935, which implies that the breach was aft of the cross spar. Because the cross spar attaches to the transition spar behind RCC panel 6, the breach must have been aft (outboard) of panel 6. The superheated air likely burned through the outboard wall of the wheel well, rather than snaking forward and then back through the vent at the front of the wheel well. Had the gases flowed through the access opening in the cross spar and then through the vent into the wheel well, it is unlikely that the lower strain gauge wiring would have survived.

Finally, the rapid rise in Sensor 4 at EI+425, before the other sensors began to fail, indicates that high temperatures were responsible. Comparisons of sensors on the outside of the wing leading edge spar, those inside of the spar, and those in the wing and left wheel well indicate that abnormal heating first began on the outside of the spar behind the RCC panels and worked through the spar. Since the aluminum spar must have burned through before any cable harnesses attached to it failed, the breach through the wing leading edge spar must have occurred at or before EI+487.

Other abnormalities also occurred during re-entry. Early in re-entry, the heating normally seen on the left Orbital Maneuvering System pod was much lower than usual for this point in the flight (see Figure 3.6-9). Wind tunnel testing demonstrated that airflow into a breach in an RCC panel would then escape through the wing leading edge vents behind the upper part of the panel and interrupt the weak aerodynamic flow field on top of the wing. During re-entry, air normally flows into these vents to equalize air pressure across the RCC panels. The interruption in the flow field behind the wing caused a displacement of the vortices that normally hit the leading edge of the left pod, and resulted in a slowing of pod heating. Heating of the side fuselage slowed, which wind tunnel testing also predicted.

To match this scenario, investigators had to postulate damage to the tiles on the upper carrier panel 9, in order to allow sufficient mass flow through the vent to cause the observed decrease in sidewall heating. No upper carrier panels were found from panels 9, 10, and 11, which supports this hypothesis. Although this can account for the abnormal temperatures on the body of the Orbiter and at the Orbital Maneuvering System pod, flight data and wind tunnel tests confirmed that this venting was not strong enough to alter the aerodynamic force on the Orbiter, and the aerodynamic analysis of mission data showed no change in Orbiter flight control parameters during this time.

During re-entry, a change was noted in the rate of the temperature rise around the RCC chin panel clevis temperature sensor and two water supply nozzles on the left side of the fuselage, just aft of the main bulkhead that divides the crew cabin from the payload bay. Because these sensors were well forward of the damage in the left wing leading edge, it is still unclear how their indications fit into the failure scenario.

### Sensor Loss and the Onset of Unusual Aerodynamic Effects (EI+500 through EI+611)

Fourteen seconds after the loss of the first sensor wire on the wing leading edge spar at EI+487, a sensor wire in a bundle of some 150 wires that ran along the upper outside corner of the left wheel well showed a burn-through. In the next 50 seconds, more than 70 percent of the sensor wires in three cables in this area also burned through (see Figure 3.6-10). Investigators plotted the wiring run for every left-wing sensor, looking for a relationship between their location and time of failure.

Only two sensor wires of 169 remained intact when the Modular Auxiliary Data System recorder stopped, indicat-

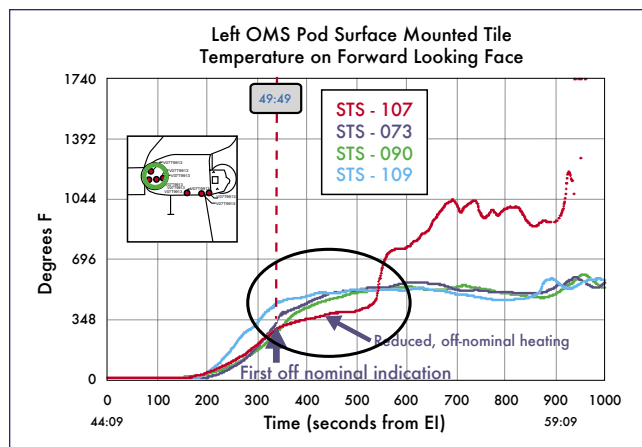


Figure 3.6-9. Orbital Maneuvering System (OMS) pod heating was initially significantly lower than that seen on previous Columbia missions. As wing leading edge damage later increased, the OMS pod heating increased dramatically. Debris recovered from this area of the OMS pod showed substantial pre-breakup heat damage and imbedded drops of once-molten metal from the wing leading edge in the OMS pod thermal tiles.

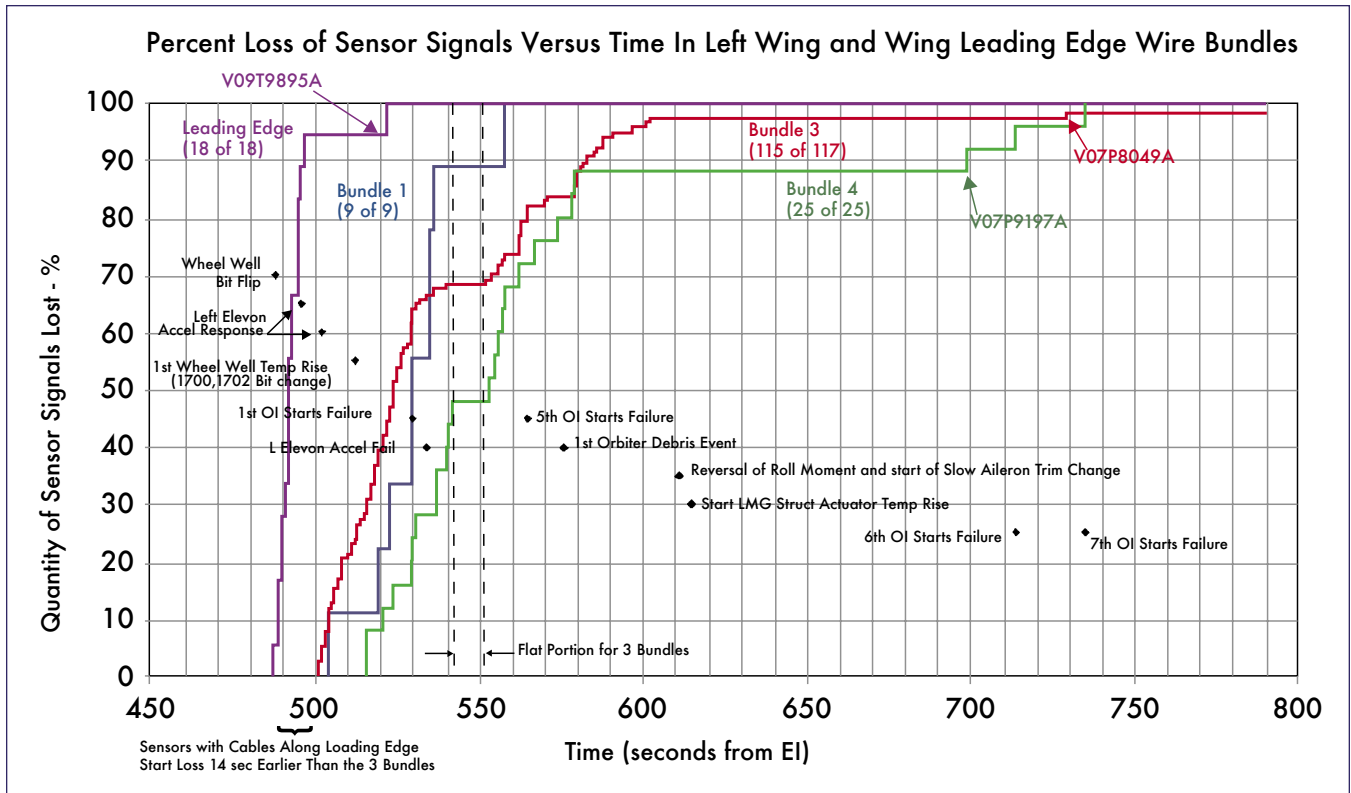


Figure 3.6-10. This chart shows how rapidly the wire bundles in the left wing were destroyed. Over 70 percent of the sensor wires in the wiring bundles burned through in under a minute. The black diamonds show the times of significant timeline sensor events.

ing that the burn-throughs had to occur in an area that nearly every wire ran through. To sustain this type of damage, the wires had to be close enough to the breach for the gas plume to hit them. Arc jet testing (in a wind tunnel with an electrical arc that provides up to a 2,800-degree Fahrenheit airflow) on a simulated wing leading edge spar and simulated wire bundles showed how the leading edge spar would burn through in a few seconds. It also showed that wire bundles would burn through in a timeframe consistent with those seen in the Modular Auxiliary Data System information and the telemetered data.

Later computational fluid dynamics analysis of the mid-wing area behind the spar showed that superheated air flowing into a breached RCC panel 8 and then interacting with the internal structure behind the RCC cavity (RCC ribs and spar insulation) would have continued through the wing leading edge spar as a jet, and would have easily allowed superheated air to traverse the 56.5 inches from the spar to the outside of the wheel well and destroy the cables (Figure 3.6-11). Controllers on the ground saw these first anomalies in the telemetry data at EI+613, when four hydraulic sensor cables that ran from the aft part of the left wing through the wiring bundles outside the wheel well failed.

Aerodynamic roll and yaw forces began to differ from those on previous flights at about EI+500 (see Figure 3.6-12). Investigators used flight data to reconstruct the aerodynamic forces acting on the Orbiter. This reconstructed data was then compared to forces seen on other similar flights of *Columbia*

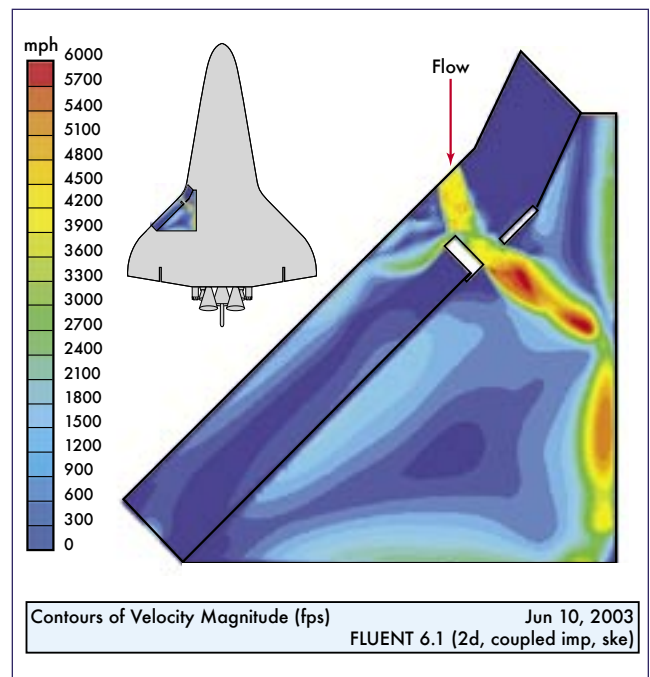


Figure 3.6-11. The computational fluid dynamics analysis of the speed of the superheated air as it entered the breach in RCC panel 8 and then traveled through the wing leading edge spar. The darkest red color indicates speeds of over 4,000 miles per hour. Temperatures in this area likely exceeded 5,000 degrees Fahrenheit. The area of detail is looking down at the top of the left wing.

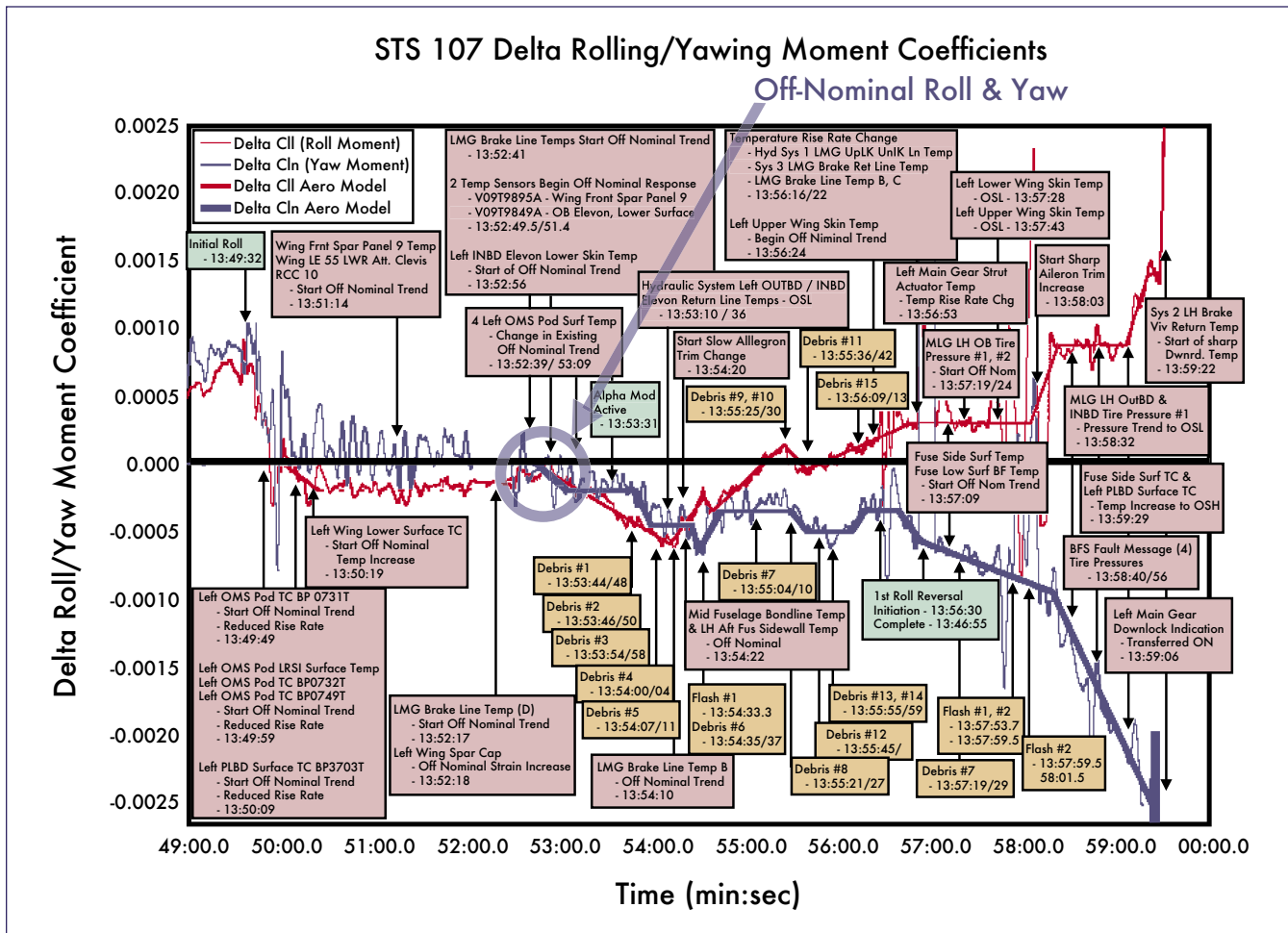


Figure 3.6-12. At approximately EI+500 seconds, the aerodynamic roll and yaw forces began to diverge from those observed on previous flights. The blue line shows the Orbiter's tendency to yaw while the red line shows its tendency to roll. Nominal values would parallel the solid black line. Above the black line, the direction of the force is to the right, while below the black line, the force is to the left.

and to the forces predicted for STS-107. In the early phase of flight, these abnormal aerodynamic forces indicated that *Columbia's* flight control system was reacting to a change in the external shape of the wing, which was caused by progressive RCC damage that caused a continuing decrease in lift and a continuing increase in drag on the left wing.

Between EI+530 and EI+562, four sensors on the left inboard elevon failed. These sensor readings were part of the data telemetered to the ground. Noting the system failures, the Maintenance, Mechanical, and Crew Systems officer notified the Flight Director of the failures. (See sidebar in Chapter 2 for a complete version of the Mission Control Center conversation about this data.)

At EI+555, *Columbia* crossed the California coast. People on the ground now saw the damage developing on the Orbiter in the form of debris being shed, and documented this with video cameras. In the next 15 seconds, temperatures on the fuselage sidewall and the left Orbital Maneuvering System pod began to rise. Hypersonic wind tunnel tests indicated that the increased heating on the Orbital Maneuvering System pod and the roll and yaw changes were caused by

substantial leading edge damage around RCC panel 9. Data on Orbiter temperature distribution as well as aerodynamic forces for various damage scenarios were obtained from wind tunnel testing.

Figure 3.6-13 shows the comparison of surface temperature distribution with an undamaged Orbiter and one with an entire panel 9 removed. With panel 9 removed, a strong vortex flow structure is positioned to increase the temperature on the leading edge of the Orbital Maneuvering System pod. The aim is not to demonstrate that all of panel 9 was missing at this point, but rather to indicate that major damage to panels near panel 9 can shift the strong vortex flow pattern and change the Orbiter's temperature distribution to match the Modular Auxiliary Data System information. Wind tunnel tests also demonstrated that increasing damage to leading edge RCC panels would result in increasing drag and decreasing lift on the left wing.

Recovered debris showed that Inconel 718, which is only found in wing leading edge spanner beams and attachment fittings, was deposited on the left Orbital Maneuvering System pod, verifying that airflow through the breach and out

of the upper slot carried molten wing leading edge material back to the pod. Temperatures far exceeded those seen on previous re-entries and further confirmed that the wing leading-edge damage was increasing.

By this time, superheated air had been entering the wing since EI+487, and significant internal damage had probably occurred. The major internal support structure in the mid-wing consists of aluminum trusses with a melting point of 1,200 degrees Fahrenheit. Because the ingested air may have been as hot as 8,000 degrees near the breach, it is likely that the internal support structure that maintains the shape of the wing was severely compromised.

As the Orbiter flew east, people on the ground continued to record the major shedding of debris. Investigators later scrutinized these videos to compare *Columbia's* re-entry with recordings of other re-entries and to identify the debris. The video analysis was also used to determine additional search areas on the ground and to estimate the size of various pieces of debris as they fell from the Orbiter.

Temperatures in the wheel well began to rise rapidly at EI+601, which indicated that the superheated air coming through the wing leading edge spar had breached the wheel well wall. At the same time, observers on the ground noted additional significant shedding of debris. Analysis of one of these "debris events" showed that the photographed object could have weighed nearly 190 pounds, which would have significantly altered *Columbia's* physical condition.

At EI+602, the tendency of the Orbiter to roll to the left in response to a loss of lift on the left wing transitioned to a right-rolling tendency, now in response to increased lift on the left wing. Observers on the ground noted additional significant shedding of debris in the next 30 seconds. Left yaw continued to increase, consistent with increasing drag on the left wing. Further damage to the RCC panels explains the increased drag on the left wing, but it does not explain the sudden increase in lift, which can be explained only by some other type of wing damage.

Investigators ran multiple analyses and wind tunnel tests to understand this significant aerodynamic event. Analysis showed that by EI+850, the temperatures inside the wing

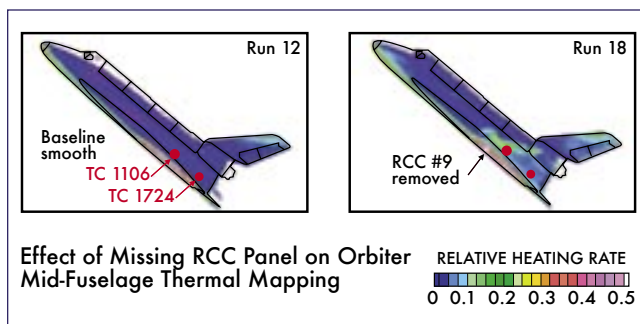
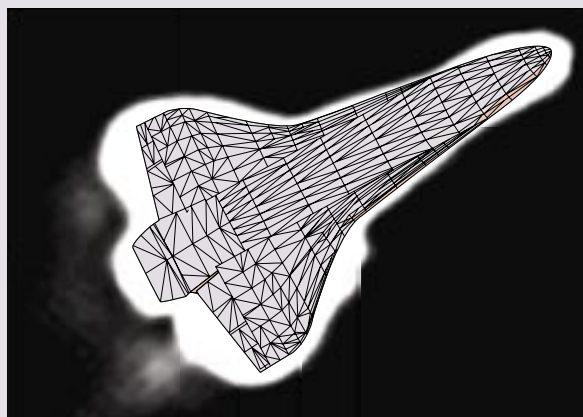


Figure 3.6-13. The effects of removing RCC panel 9 are shown in this figure. Note the brighter colors on the front of the OMS pod show increased heating, a phenomenon supported by both the OMS pod temperature sensors and the debris analysis.

## THE KIRTLAND IMAGE

As *Columbia* passed over Albuquerque, New Mexico, during re-entry (around EI+795), scientists at the Air Force Starfire Optical Range at Kirtland Air Force Base acquired images of the Orbiter. This imaging had not been officially assigned, and the photograph was taken using commercial equipment located at the site, not with the advanced Starfire adaptive-optics telescope.



The image shows an unusual condition on the left wing, a leading-edge disturbance that might indicate damage. Several analysts concluded that the distortion evident in the image likely came from the modification and interaction of shock waves due to the damaged leading edge. The overall appearance of the leading-edge damage at this point on the trajectory is consistent with the scenario.

were high enough to substantially damage the wing skins, wing leading edge spar, and the wheel well wall, and melt the wing's support struts. Once structural support was lost, the wing likely deformed, effectively changing shape and resulting in increased lift and a corresponding increase in drag on the left wing. The increased drag on the left wing further increased the Orbiter's tendency to yaw left.

## Loss of Vehicle Control (EI+612 through EI+970)

A rise in hydraulic line temperatures inside the left wheel well indicated that superheated air had penetrated the wheel well wall by EI+727. This temperature rise, telemetered to Mission Control, was noted by the Maintenance, Mechanical, and Crew Systems officer. The Orbiter initiated and completed its roll reversal by EI+766 and was positioned left-wing-down for this portion of re-entry. The Guidance and Flight Control Systems performed normally, although the aero-control surfaces (aileron trim) continued to counteract the additional drag and lift from the left wing.

At EI+790, two left main gear outboard tire pressure sensors began trending slightly upward, followed very shortly by going off-scale low, which indicated extreme heating of both the left inboard and outboard tires. The tires, with their large mass, would require substantial heating to produce the sensors' slight temperature rise. Another sharp change in the rolling tendency of the Orbiter occurred at EI+834, along

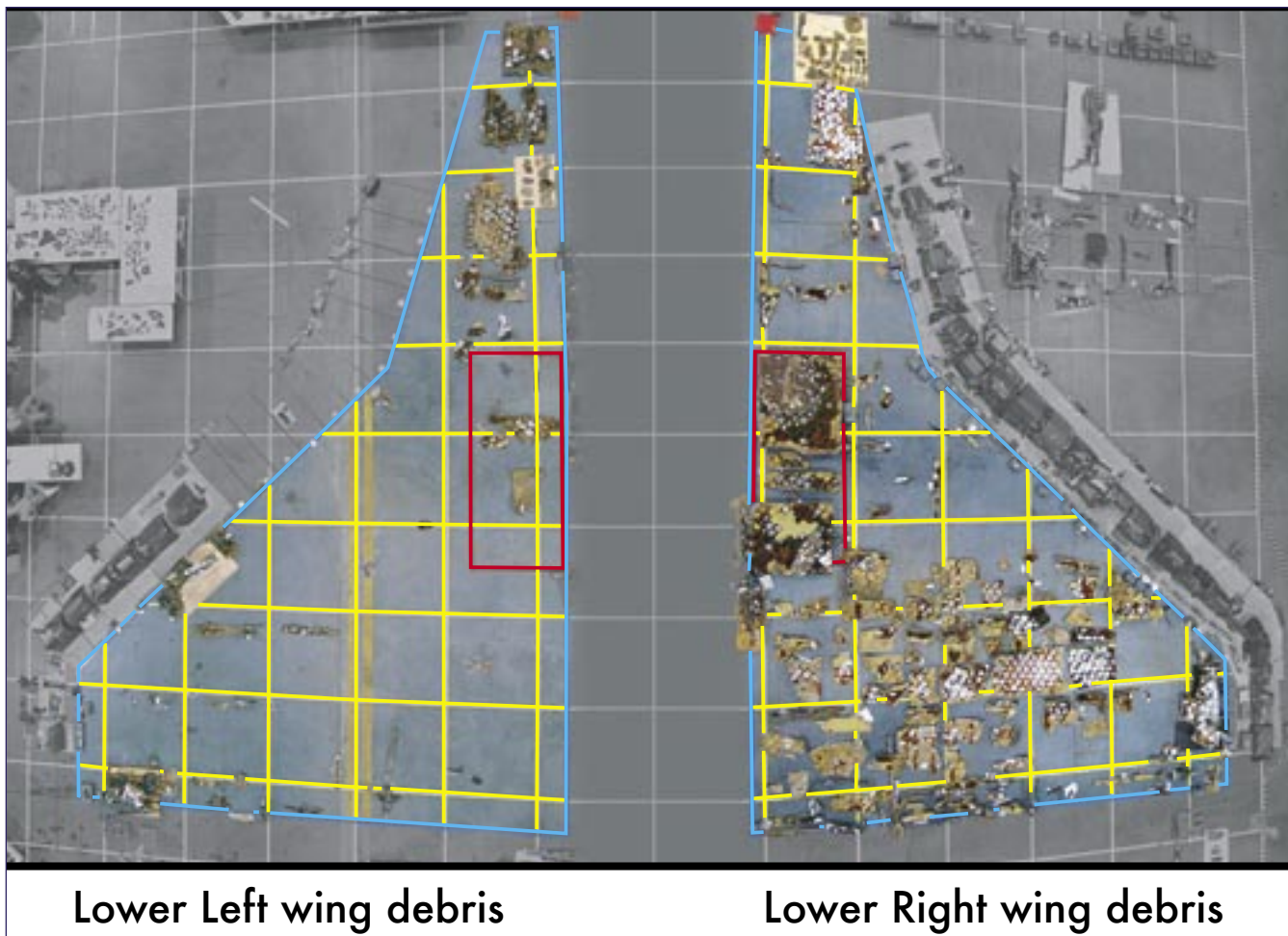


Figure 3.7-1. Comparison of amount of debris recovered from the left and right wings of Columbia. Note the amount of debris recovered from areas in front of the wheel well (the red boxes on each wing) were similar, but there were dramatic differences in the amount of debris recovered aft of each wheel well.

with additional shedding of debris. In an attempt to maintain attitude control, the Orbiter responded with a sharp change in aileron trim, which indicated there was another significant change to the left wing configuration, likely due to wing deformation. By EI+887, all left main gear inboard and outboard tire pressure and wheel temperature measurements were lost, indicating burning wires and a rapid progression of damage in the wheel well.

At EI+897, the left main landing gear downlock position indicator reported that the gear was now down and locked. At the same time, a sensor indicated the landing gear door was still closed, while another sensor indicated that the main landing gear was still locked in the up position. Wire burn-through testing showed that a burn-induced short in the downlock sensor wiring could produce these same contradictions in gear status indication. Several measurements on the strut produced valid data until the final loss of telemetry data. This suggests that the gear-down-and locked indication was the result of a wire burn-through, not a result of the landing gear actually deploying. All four corresponding proximity switch sensors for the right main landing gear remained normal throughout re-entry until telemetry was lost.

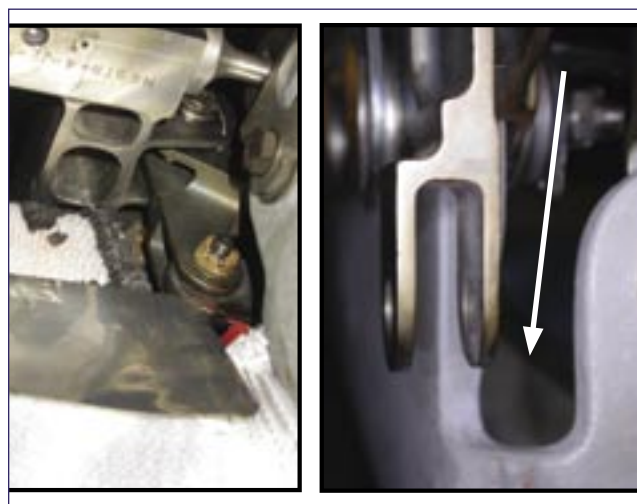


Figure 3.7-2. Each RCC panel has a U-shaped slot (see arrow) in the back of the panel. Once superheated air entered the breach in RCC panel 8, some of that superheated air went through this slot and caused substantial damage to the Thermal Protection System tiles behind this area.

Post-accident analysis of flight data that was generated after telemetry information was lost showed another abrupt change in the Orbiter's aerodynamics caused by a continued progression of left wing damage at EI+917. The data showed a significant increase in positive roll and negative yaw, again indicating another increase in drag on and lift from the damaged left wing. *Columbia's* flight control system attempted to compensate for this increased left yaw by firing all four right yaw jets. Even with all thrusters firing, combined with a maximum rate of change of aileron trim, the flight control system was unable to control the left yaw, and control of the Orbiter was lost at EI+970 seconds. Mission Control lost all telemetry data from the Orbiter at EI+923 (8:59:32 a.m.). Civilian and military video cameras on the ground documented the final breakup. The Modular Auxiliary Data System stopped recording at EI+970 seconds.

**Findings:**

- F3.6-1 The de-orbit burn and re-entry flight path were normal until just before Loss of Signal.
- F3.6-2 *Columbia* re-entered the atmosphere with a pre-existing breach in the left wing.
- F3.6-3 Data from the Modular Auxiliary Data System recorder indicates the location of the breach was in the RCC panels on the left wing leading edge.
- F3.6-4 Abnormal heating events preceded abnormal aerodynamic events by several minutes.
- F3.6-5 By the time data indicating problems was telemetered to Mission Control Center, the Orbiter had already suffered damage from which it could not recover.

**Recommendations:**

- R3.6-1 The Modular Auxiliary Data System instrumentation and sensor suite on each Orbiter should be maintained and updated to include current sensor and data acquisition technologies.
- R3.6-2 The Modular Auxiliary Data System should be redesigned to include engineering performance and vehicle health information, and have the ability to be reconfigured during flight in order to allow certain data to be recorded, telemetered, or both, as needs change.

**3.7 DEBRIS ANALYSIS**

The Board performed a detailed and exhaustive investigation of the debris that was recovered. While sensor data from the Orbiter pointed to early problems on the left wing, it could only isolate the breach to the general area of the left wing RCC panels. Forensics analysis independently determined that RCC panel 8 was the most likely site of the breach, and this was subsequently corroborated by other analyses. (See Appendix D.11.)

**Pre-Breakup and Post-Breakup Damage Determination**

Differentiating between pre-breakup and post-breakup damage proved a challenge. When *Columbia's* main body break-

up occurred, the Orbiter was at an altitude of about 200,000 feet and traveling at Mach 19, well within the peak-heating region calculated for its re-entry profile. Consequently, as individual pieces of the Orbiter were exposed to the atmosphere at breakup, they experienced temperatures high enough to damage them. If a part had been damaged by heat prior to breakup, high post-breakup temperatures could easily conceal the pre-breakup evidence. In some cases, there was no clear way to determine what happened when. In other cases, heat erosion occurred over fracture surfaces, indicating the piece had first broken and had then experienced high temperatures. Investigators concluded that pre- and post-breakup damage had to be determined on a part-by-part basis; it was impossible to make broad generalizations based on the gross physical evidence.

**Amount of Right Wing Debris versus Left Wing Debris**

Detailed analysis of the debris revealed unique features and convincing evidence that the damage to the left wing differed significantly from damage to the right, and that significant differences existed in pieces from various areas of the left wing. While a substantial amount of upper and lower right wing structure was recovered, comparatively little of the upper and lower left wing structure was recovered (see Figure 3.7-1).

The difference in recovered debris from the Orbiter's wings clearly indicates that after the breakup, most of the left wing succumbed to both high heat and aerodynamic forces, while the right wing succumbed to aerodynamic forces only. Because the left wing was already compromised, it was the first area of the Orbiter to fail structurally. Pieces were exposed to higher heating for a longer period, resulting in more heat damage and ablation of left wing structural material. The left wing was also subjected to superheated air that penetrated directly into the mid-body of the wing for a substantial period. This pre-heating likely rendered those components unable to absorb much, if any, of the post-breakup heating. Those internal and external structures were likely vaporized during post-breakup re-entry. Finally, the left wing likely lost significant amounts of the Thermal Protection System prior to breakup due to the effect of internal wing heating on the Thermal Protection System bonding materials, and this further degraded the left wing's ability to resist the high heat of re-entry after it broke up.

**Tile Slumping and External Patterns of Tile Loss**

Tiles recovered from the lower left wing yielded their own interesting clues. The left wing lower carrier panel 9 tiles sustained extreme heat damage (slumping) and showed more signs of erosion than any other tiles. This severe heat erosion damage was likely caused by an *outflow* of superheated air and molten material from behind RCC panel 8 through a U-shaped design gap in the panel (see Figure 3.7-2) that allows room for the T-seal attachment. Effluents from the back side of panel 8 would directly impact this area of lower carrier panel 9 and its tiles. In addition, flow lines in these tiles (see Figure 3.7-3) exhibit evidence of superheated airflow across their surface from the area of the RCC panel

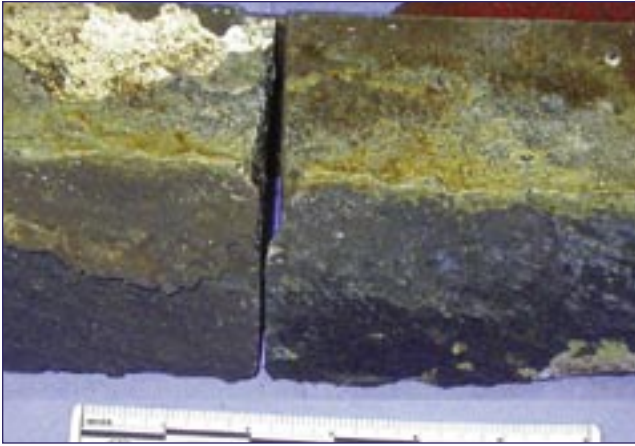


Figure 3.7-3. Superheated airflow caused erosion in tiles around the RCC panel 8 and 9 interface. The tiles shown are from behind the area where the superheated air exited from the slot in Figure 3.7-2. These tiles showed much greater thermal damage than other tiles in this area and chemical analysis showed the presence of metals only found in wing leading edge components.

8 and 9 interface. Chemical analysis shows that these carrier panel tiles were covered with molten Inconel, which is found in wing leading edge attachment fittings, and other metals coming from inside the RCC cavity. Slumping and heavy erosion of this magnitude is not noted on tiles from anywhere else on the Orbiter.

Failure modes of recovered tiles from the left and the right wing also differ. Most right wing tiles were simply broken off the wing due to aerodynamic forces, which indicates that they failed due to physical overload at breakup, not because of heat. Most of the tiles on the left wing behind RCC panels 8 and 9 show significant evidence of backside heating of the wing skin and failure of the adhesive that held the tiles on the wing. This pattern of failure suggests that heat penetrated the left wing cavity and then heated the aluminum skin from the inside out. As the aluminum skin was heated,

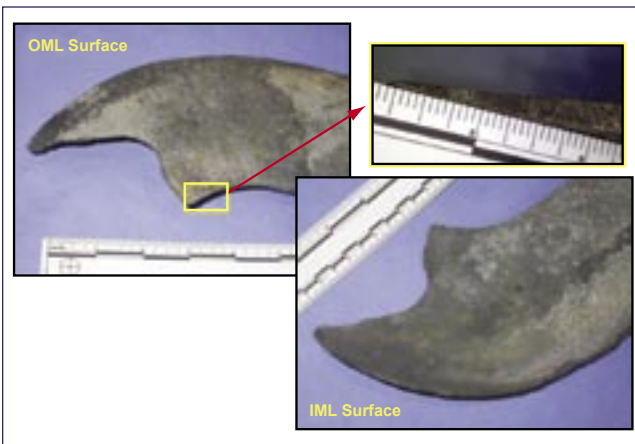


Figure 3.7-4. The outboard rib of panel 8 and the inboard rib of panel 9 showed signs of extreme heating and erosion. RCC erosion of this magnitude was not observed in any other location on the Orbiter.

the strength of the tile bond degraded, and tiles separated from the Orbiter.

### Erosion of Left Wing Reinforced Carbon-Carbon

Several pieces of left wing RCC showed unique signs of heavy erosion from exposure to extreme heat. There was erosion on two rib panels on the left wing leading edge in the RCC panel 8 and 9 interface. Both the outboard rib of panel 8 and the inboard rib of panel 9 showed signs of extreme heating and erosion (see Figure 3.7-4). This erosion indicates that there was extreme heat behind RCC panels 8 and 9. This type of RCC erosion was not seen on any other part of the left or right wing.

### Locations of Reinforced Carbon-Carbon Debris

The location of debris on the ground also provided evidence of where the initial breach occurred. The location of every piece of recovered RCC was plotted on a map and labeled according to the panel the piece originally came from. Two distinct patterns were immediately evident. First, it was clear that pieces from left wing RCC panels 9 through 22 had fallen the farthest west, and that RCC from left wing panels 1 through 7 had fallen considerably farther east (see Figure 3.7-5). Second, pieces from left wing panel 8 were

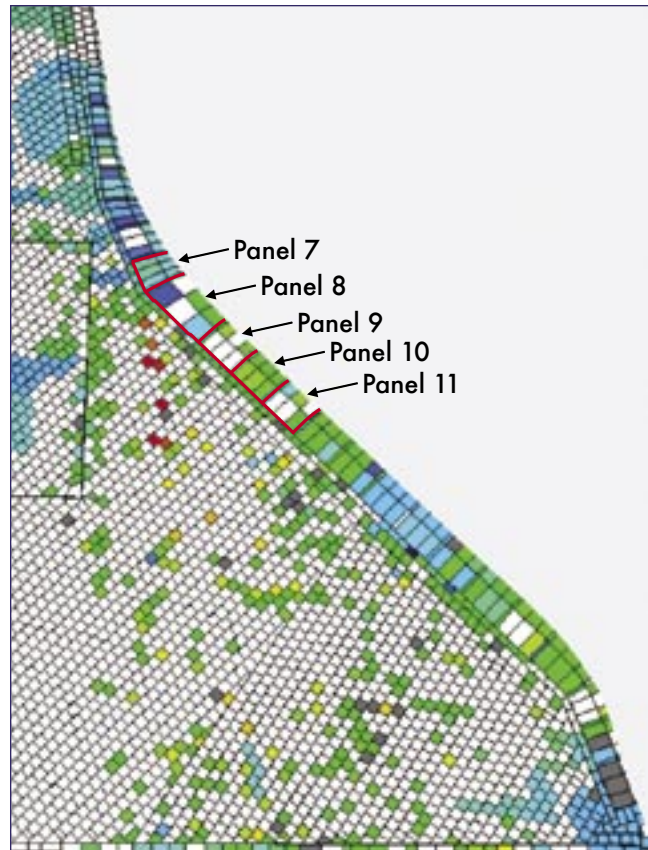


Figure 3.7-6. The tiles recovered farthest west all came from the area immediately behind left wing RCC panels 8 and 9. In the figure, each small box represents an individual tile on the lower surface of the left wing. The more red an individual tile appears, the farther west it was found.

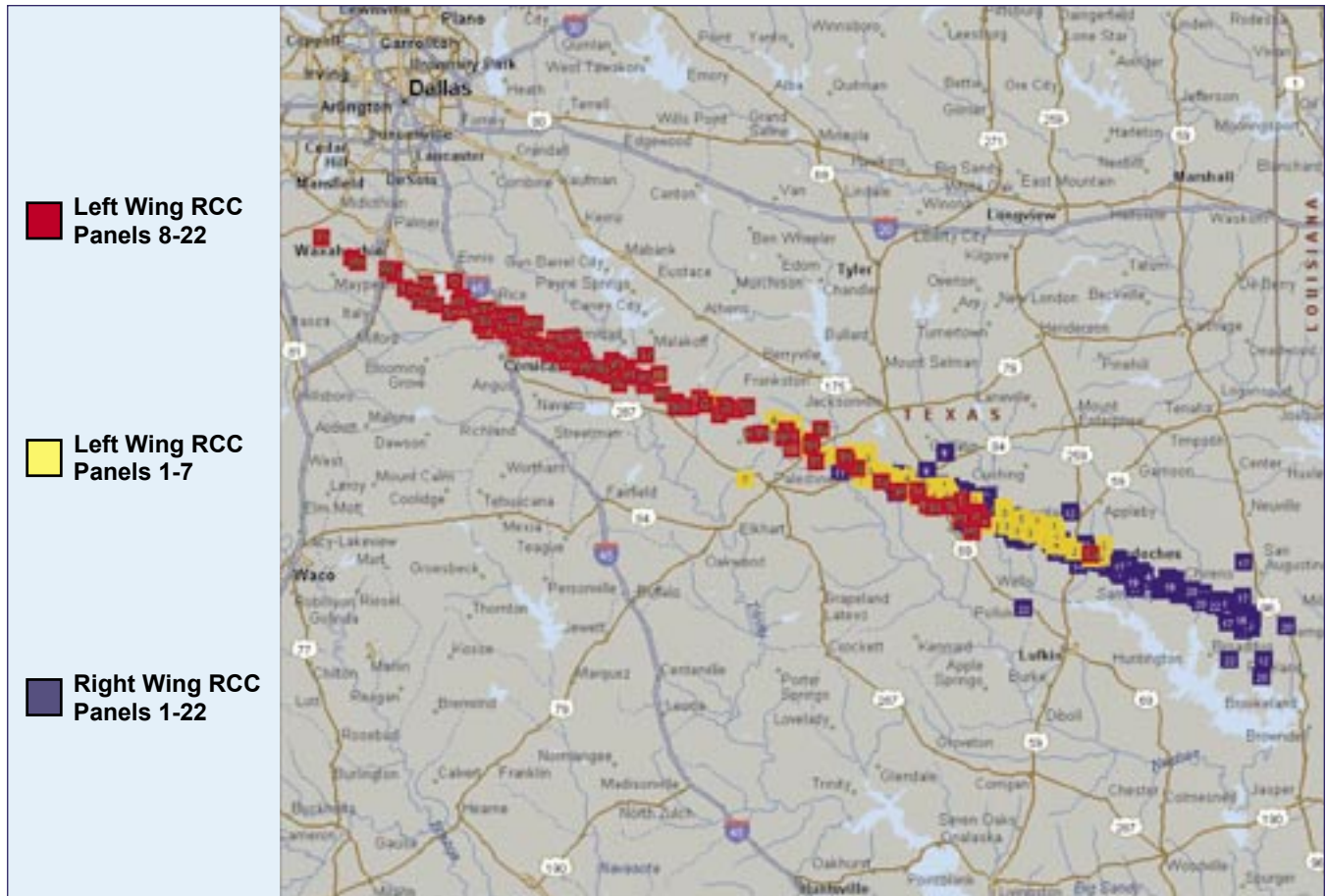


Figure 3.7-5. The location of RCC panel debris from the left and right wings, shown where it was recovered from in East Texas. The debris pattern suggested that the left wing failed before the right wing, most likely near left RCC panels 8 and 9.

found throughout the debris field, which suggested that the left wing likely failed in the vicinity of RCC panel 8. The early loss of the left wing from RCC panel 9 and outboard caused the RCC from that area to be deposited well west of the RCC from the inboard part of the wing. Since panels 1 through 7 were so much farther to the east, investigators concluded that RCC panels 1 through 7 had stayed with the Orbiter longer than had panels 8 through 22.

#### Tile Locations

An analysis of where tiles were found on the ground also yielded significant evidence of the breach location. Since most of the tiles are of similar size, weight, and shape, they would all have similar ballistic coefficients and would have behaved similarly after they separated from the Orbiter. By noting where each tile fell and then plotting its location on the Orbiter tile map, a distinctive pattern emerged. The tiles recovered farthest west all came from the area immediately behind the left wing RCC panel 8 and 9 (see Figure 3.7-6), which suggests that these tiles were released earlier than those from other areas of the left wing. While it is not conclusive evidence of a breach in this area, this pattern does suggest unique damage around RCC panels 8 and 9 that was not seen in other areas. Tiles from this area also showed evidence of a brown deposit that was not seen on tiles from any

other part of the Orbiter. Chemical analysis revealed it was an Inconel-based deposit that had come from inside the RCC cavity on the left wing (Inconel is found in wing leading edge attachment fittings). Since the streamlines from tiles with the brown deposit originate near left RCC panels 8 and 9, this brown deposit likely originated as an outflow of superheated air and molten metal from the panel 8 and 9 area.

#### Molten Deposits

High heat damage to metal parts caused molten deposits to form on some Orbiter debris. Early analysis of these deposits focused on their density and location. Much of the left wing leading edge showed some signs of deposits, but the left wing RCC panels 5 to 10 had the highest levels.

Of all the debris pieces recovered, left wing panels 8 and 9 showed the largest amounts of deposits. Significant but lesser amounts of deposits were also observed on left wing RCC panels 5 and 7. Right wing RCC panel 8 was the only right-wing panel with significant deposits.

#### Chemical and X-Ray Analysis

Chemical analysis focused on recovered pieces of RCC panels with unusual deposits. Samples were obtained from areas

in the vicinity of left wing RCC panel 8 as well as other left and right wing RCC panels. Deposits on recovered RCC debris were analyzed by cross-sectional optical and scanning electron microscopy, microprobe analysis, and x-ray diffraction to determine the content and layering of slag deposits. Slag was defined as metallic and non-metallic deposits that resulted from the melting of the internal wing structures. X-ray analysis determined the best areas to sample for chemical testing and to see if an overall flow pattern could be discerned.

The X-ray analysis of left wing RCC panel 8 (see Figure 3.7-7) showed a bottom-to-top pattern of slag deposits. In some areas, small spheroids of heavy metal were aligned vertically on the recovered pieces, which indicated a superheated airflow from the bottom of the panel toward the top in the area of RCC panel 8-left. These deposits were later determined by chemical analysis to be Inconel 718, probably from the wing leading edge attachment fittings on the spanner beams on RCC panels 8 and 9. Computational fluid dynamics modeling of the flow behind panel 8 indicated that the molten deposits would be laid down in this manner.

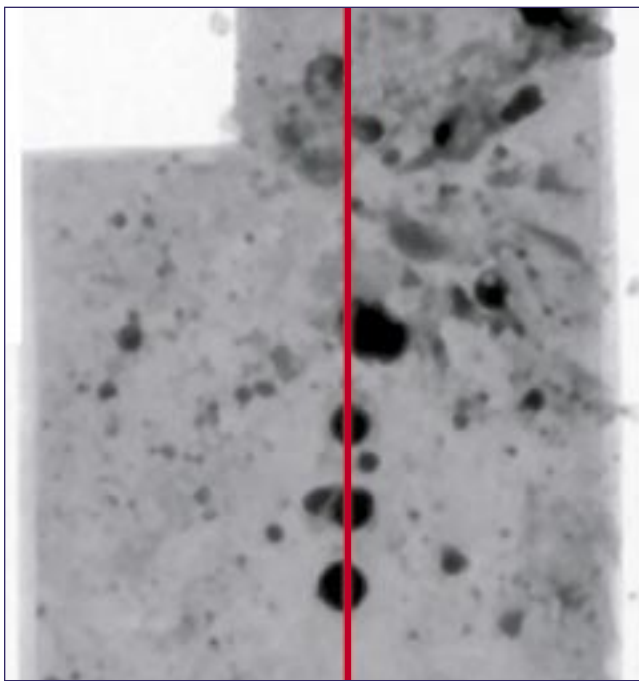


*Figure 3.7-7. X-ray analysis of RCC panel 8-left showed a bottom-to-top pattern of slag deposits.*

The layered deposits on panel 8 were also markedly different from those on all other left- and right-wing panels. There was much more material deposited on RCC panel 8-left. These deposits had a much rougher overall structure, including rivulets of Cerachrome slag deposited directly on the RCC. This indicated that Cerachrome, the insulation that protects the wing leading edge spar, was one of the first materials to succumb to the superheated air entering through the breach in RCC panel 8-left. Because the melting temperature of Cerachrome is greater than 3,200 degrees Fahrenheit, analysis indicated that materials in this area were exposed to extremely

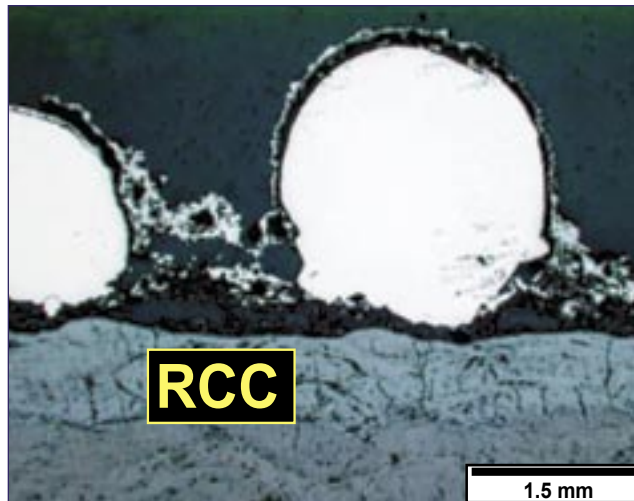


*Figure 3.7-8. Spheroids of Inconel 718 and Cerachrome were deposited directly on the surface of RCC panel 8-left. This slag deposit pattern was not seen on any other RCC panels.*

high temperatures for a long period. Spheroids of Inconel 718 were mixed in with the Cerachrome. Because these spheroids (see Figure 3.7-8) were directly on the surface of the RCC and also in the first layers of deposits, investigators concluded that the Inconel 718 spanner beam RCC fittings were most likely the first internal structures subjected to intense heating. No aluminum was detected in the earliest slag layers on RCC panel 8-left. Only one location on an upper corner piece, near the spar fitting attachment, contained A-286 stainless steel. This steel was not present in the bottom layer of the slag directly on the RCC surface, which indicated that the A-286 attachment fittings on the wing spar were not in the direct line of the initial plume impingement.

In wing locations other than left RCC panels 8 and 9, the deposits were generally thinner and relatively uniform. This suggests no particular breach location other than in left RCC panels 8 and 9. These other slag deposits contained primarily aluminum and aluminum oxides mixed with A-286, Inconel, and Cerachrome, with no consistent layering. This mixing of multiple metals in no apparent order suggests concurrent melting and re-depositing of all leading-edge components, which is more consistent with post-breakup damage than the organized melting and depositing of materials that occurred near the original breach at left RCC panels 8 and 9. RCC panel 9-left also differs from the rest of the locations analyzed. It was similar to panel 8-left on the inboard side, but more like the remainder of the samples analyzed on its outboard side. The deposition of molten deposits strongly suggests the original breach occurred in RCC panel 8-left.

### **Spanner Beams, Fittings, and Upper Carrier Panels**

Spanner beams, fittings, and upper carrier panels were recovered from areas adjacent to most of the RCC panels on both wings. However, significant numbers of these items were not recovered from the vicinity of left RCC panels 6 to 10. None of the left wing upper carrier panels at positions 9, 10, or 11 were recovered. No spanner beam parts were recovered from

## STS-107 CREW SURVIVABILITY

At the Board's request, NASA formed a Crew Survivability Working Group within two weeks of the accident to better understand the cause of crew death and the breakup of the crew module. This group made the following observations.

### Medical and Life Sciences

The Working Group found no irregularities in its extensive review of all applicable medical records and crew health data. The Armed Forces Institute of Pathology and the Federal Bureau of Investigation conducted forensic analyses on the remains of the crew of *Columbia* after they were recovered. It was determined that the acceleration levels the crew module experienced prior to its catastrophic failure were not lethal. The death of the crew members was due to blunt trauma and hypoxia. The exact time of death – sometime after 9:00:19 a.m. Eastern Standard Time – cannot be determined because of the lack of direct physical or recorded evidence.

### Failure of the Crew Module

The forensic evaluation of all recovered crew module/forward fuselage components did not show any evidence of over-pressurization or explosion. This conclusion is supported by both the lack of forensic evidence and a credible source for either sort of event.<sup>11</sup> The failure of the crew module resulted from the thermal degradation of structural properties, which resulted in a rapid catastrophic sequential structural breakdown rather than an instantaneous "explosive" failure.

Separation of the crew module/forward fuselage assembly from the rest of the Orbiter likely occurred immediately in front of the payload bay (between Xo576 and Xo582 bulkheads). Subsequent breakup of the assembly was a result of ballistic heating

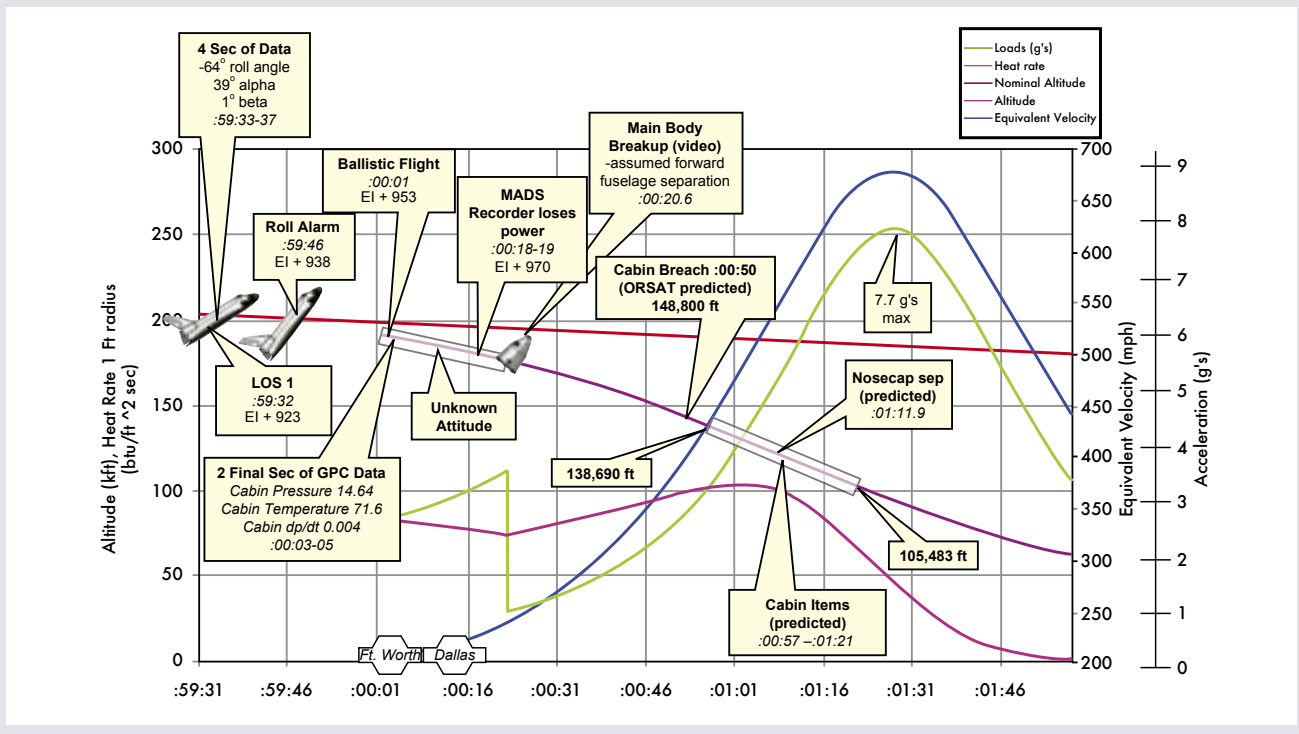
and dynamic loading. Evaluations of fractures on both primary and secondary structure elements suggest that structural failures occurred at high temperatures and in some cases at high strain rates. An extensive trajectory reconstruction established the most likely breakup sequence, shown below.

The load and heat rate calculations are shown for the crew module along its reconstructed trajectory. The band superimposed on the trajectory (starting about 9:00:58 a.m. EST) represents the window where all the evaluated debris originated. It appears that the destruction of the crew module took place over a period of 24 seconds beginning at an altitude of approximately 140,000 feet and ending at 105,000 feet. These figures are consistent with the results of independent thermal re-entry and aerodynamic models. The debris footprint proved consistent with the results of these trajectory analyses and models. Approximately 40 to 50 percent, by weight, of the crew module was recovered.

The Working Group's results significantly add to the knowledge gained from the loss of *Challenger* in 1986. Such knowledge is critical to efforts to improve crew survivability when designing new vehicles and identifying feasible improvements to the existing Orbiters.

### Crew Worn Equipment

Videos of the crew during re-entry that have been made public demonstrate that prescribed procedures for use of equipment such as full-pressure suits, gloves, and helmets were not strictly followed. This is confirmed by the Working Group's conclusions that three crew members were not wearing gloves, and one was not wearing a helmet. However, under these circumstances, this did not affect their chances of survival.



## BOARD TESTING

NASA and the Board agreed that tests would be required and a test plan developed to validate an impact/breach scenario. Initially, the Board intended to act only in an oversight role in the development and implementation of a test plan. However, ongoing and continually unresolved debate on the size and velocity of the foam projectile, largely due to the Marshall Space Flight Center's insistence that, despite overwhelming evidence to the contrary, the foam could have been no larger than 855 cubic inches, convinced the Board to take a more active role. Additionally, in its assessment of potential foam damage NASA continued to rely heavily on the Crater model, which was used during the mission to determine that the foam-shedding event was non-threatening. Crater is a semi-empirical model constructed from Apollo-era data. Another factor that contributed to the Board's decision to play an active role in the test program was the Orbiter Vehicle Engineering Working Group's requirement that the test program be used to validate the Crater model. NASA failed to focus on physics-based pre-test predictions, the schedule priorities for RCC tests that were determined by transport analysis, the addition of appropriate test instrumentation, and the consideration of additional factors such as launch loads. Ultimately, in discussions with the Orbiter Vehicle Engineering Working Group and the NASA Accident Investigation Team, the Board provided test plan requirements that outlined the template for all testing. The Board directed that a detailed written test plan, with Board-signature approval, be provided before each test.

the left RCC panel 8 to 10 area. No upper or lower RCC fittings were recovered for left panels 8, 9, or 10. Some of this debris may not have been found in the search, but it is unlikely that all of it was missed. Much of this structure probably melted, and was burned away by superheated air inside the wing. What did not melt was so hot that when it broke apart, it did not survive the heat of re-entry. This supports the theory that superheated air penetrated the wing in the general area of RCC panel 8-left and caused considerable structural damage to the left wing leading edge spar and hardware.

### Debris Analysis Conclusions

A thorough analysis of left wing debris (independent of the preceding aerodynamic, aerothermal, sensor, and photo data) supports the conclusion that significant abnormalities occurred in the vicinity of left RCC panels 8 and 9. The preponderance of debris evidence alone strongly indicates that the breach occurred in the bottom of panel 8-left. The unique composition of the slag found in panels 8 and 9, and especially on RCC panel 8-left, indicates extreme and prolonged heating in these areas very early in re-entry.

The early loss of tiles in the region directly behind left RCC panels 8 and 9 also supports the conclusion that a breach through the wing leading edge spar occurred here. This allowed superheated air to flow into the wing directly behind panel 8. The heating of the aluminum wing skin degraded tile adhesion and contributed to the early loss of tiles.

Severe damage to the lower carrier panel 9-left tiles is indicative of a flow out of panel 8-left, also strongly sug-

gesting that the breach in the RCC was through panel 8-left. It is noteworthy that it occurred only in this area and not in any other areas on either the left or the right wing lower carrier panels. There is also significant and unique evidence of severe "knife edges" erosion in left RCC panels 8 and 9. Lastly, the pattern of the debris field also suggests the left wing likely failed in the area of RCC panel 8-left.

The preponderance of unique debris evidence in and near RCC panel 8-left strongly suggests that a breach occurred here. Finally, the unique debris damage in the RCC panel 8-left area is completely consistent with other data, such as the Modular Auxiliary Data System recorder, visual imagery analysis, and the aerodynamic and aerothermal analysis.

### Findings:

- F3.7-1 Multiple indications from the debris analysis establish the point of heat intrusion as RCC panel 8-left.
- F3.7-2 The recovery of debris from the ground and its reconstruction was critical to understanding the accident scenario.

### Recommendations:

- None

## 3.8 IMPACT ANALYSIS AND TESTING

The importance of understanding this potential impact damage and the need to prove or disprove the impression that foam could not break an RCC panel prompted the investigation to develop computer models for foam impacts and undertake an impact-testing program of shooting pieces of foam at a mockup of the wing leading edge to re-create, to the extent practical, the actual STS-107 debris impact event.

Based on imagery analysis conducted during the mission and early in the investigation, the test plan included impacts on the lower wing tile, the left main landing gear door, the wing leading edge, and the carrier panels.

A main landing gear door assembly was the first unit ready for testing. By the time that testing occurred, however, analysis was pointing to an impact site in RCC panels 6 through 9. After the main landing gear door tests, the analysis and testing effort shifted to the wing leading edge RCC panel assemblies. The main landing gear door testing provided valuable data on test processes, equipment, and instrumentation. Insignificant tile damage was observed at the low impact angles of less than 20 degrees (the impact angle if the foam had struck the main landing gear door would have been roughly five degrees). The apparent damage threshold was consistent with previous testing with much smaller projectiles in 1999, and with independent modeling by Southwest Research Institute. (See Appendix D.12.)

### Impact Test – Wing Leading Edge Panel Assemblies

The test concept was to impact flightworthy wing leading edge RCC panel assemblies with a foam projectile fired by

a compressed-gas gun. Target panel assemblies with a flight history similar to *Columbia's* would be mounted on a support that was structurally equivalent to *Columbia's* wing. The attaching hardware and fittings would be either flight certified or built to *Columbia* drawings. Several considerations influenced the overall RCC test design:

- RCC panel assemblies were limited, particularly those with a flight history similar to *Columbia's*.
- The basic material properties of new RCC were known to be highly variable and were not characterized for high strain rate loadings typical of an impact.
- The influence of aging was uncertain.
- The RCC's brittleness allowed only one test impact on each panel to avoid the possibility that hidden damage would influence the results of later impacts.
- The structural system response of RCC components, their support hardware, and the wing structure was complex.
- The foam projectile had to be precisely targeted, because the predicted structural response depended on the impact point.

Because of these concerns, engineering tests with fiberglass panel assemblies from the first Orbiter, *Enterprise*,<sup>12</sup> were used to obtain an understanding of overall system response to various impact angles, locations, and foam orientations. The fiberglass panel impact tests were used to confirm instrumentation design and placement and the adequacy of the overall test setup.

Test projectiles were made from the same type of foam as the bipod ramp on STS-107's External Tank. The projectile's mass and velocity were determined by the previously described "best fit" image and transport analyses. Because the precise impact point was estimated, the aiming point for any individual test panel was based on structural analyses to maximize the loads in the area being assessed without producing a spray of foam over the top of the wing. The angle of impact relative to the test panel was determined from

the transport analysis of the panel being tested. The foam's rotational velocity was accounted for with a three-degree increase in the impact angle.

### Computer Modeling of Impact Tests

The investigation used sophisticated computer models to analyze the foam impact and to help develop an impact test program. Because an exhaustive test matrix to cover all feasible impact scenarios was not practical, these models were especially important to the investigation.

The investigation impact modeling team included members from Boeing, Glenn Research Center, Johnson Space Center, Langley Research Center, Marshall Space Flight Center, Sandia National Laboratory, and Stellingwerf Consulting. The Board also contracted with Southwest Research Institute to perform independent computer analyses because of the institute's extensive test and analysis experience with ballistic impacts, including work on the Orbiter's Thermal Protection System. (Appendix D.12 provides a complete description of Southwest's impact modeling methods and results.)

The objectives of the modeling effort included (1) evaluation of test instrumentation requirements to provide test data with which to calibrate the computer models, (2) prediction of stress, damage, and instrumentation response prior to the Test Readiness Reviews, and (3) determination of the flight conditions/loads (vibrations, aerodynamic, inertial, acoustic, and thermal) to include in the tests. In addition, the impact modeling team provided information about foam impact locations, orientation at impact, and impact angle adjustments that accounted for the foam's rotational velocity.

### Flight Environment

A comprehensive consideration of the Shuttle's flight environment, including temperature, pressure, and vibration, was required to establish the experimental protocol.

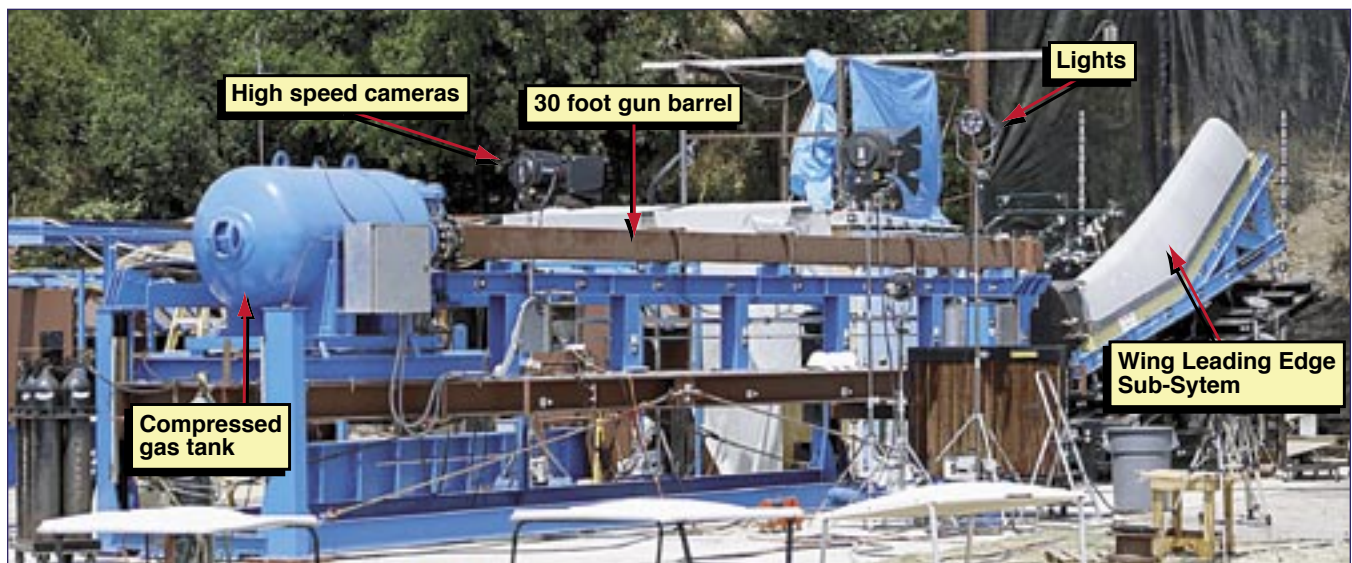


Figure 3.8-1. Nitrogen-powered gun at the Southwest Research Institute used for the test series.

Based on the results of Glenn Research Center sub-scale impact tests of how various foam temperatures and pressures influence the impact force, the Board found that full-scale impact tests with foam at room temperature and pressure could adequately simulate the conditions during the foam strike on STS-107.<sup>13</sup>

The structure of the foam complicated the testing process. The bipod ramp foam is hand-sprayed in layers, which creates “knit lines,” the boundaries between each layer, and the foam compression characteristics depend on the knit lines’ orientation. The projectiles used in the full-scale impact tests had knit lines consistent with those in the bipod ramp foam.

A primary concern of investigators was that external loads present in the flight environment might add substantial extra force to the left wing. However, analysis demonstrated that the only significant external loads on the wing leading edge structural subsystem at about 82 seconds into flight are due to random vibration and the pressure differences inside and outside the leading edge. The Board concluded that the flight environment stresses in the RCC panels and the attachment fittings could be accounted for in post-impact analyses if necessary. However, the dramatic damage produced by the impact tests demonstrated that the foam strike could breach the wing leading edge structure subsystem independent of any stresses associated with the flight environment. (Appendix D.12 contains more detail.)

### Test Assembly

The impact tests were conducted at a Southwest Research Institute facility. Figure 3.8-1 shows the nitrogen gas gun that had evaluated bird strikes on aircraft fuselages. The gun was modified to accept a 35-foot-long rectangular barrel, and the target site was equipped with sensors and high-speed cameras that photographed 2,000 to 7,000 frames per second, with intense light provided by theater spotlights and the sun.

### Test Impact Target

The leading edge structural subsystem test target was designed to accommodate the Board’s evolving determination of the

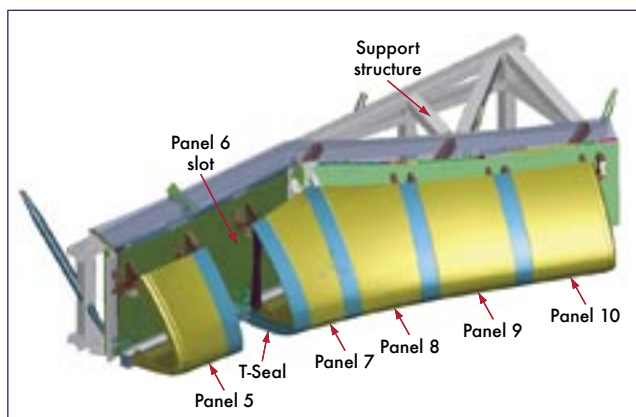


Figure 3.8-2. Test assembly that provided a structural mounting for RCC panel assemblies 5 to 10 and would accommodate some 200 sensors and other test equipment.

most likely point of impact. Initially, analysis pointed to the main landing gear door. As the imaging and transport teams refined their assessments, the likely strike zone narrowed to RCC panels 6 through 9. Because of the long lead time to develop and produce the large complex test assemblies, investigators developed an adaptable test assembly (Figure 3.8-2) that would provide a structurally similar mounting for RCC panel assemblies 5 to 10 and would accommodate some 200 sensors, including high-speed cameras, strain and deflection gauges, accelerometers, and load cells.<sup>14</sup>

### Test Panels

RCC panels 6 and 9, which bracketed the likely impact region, were the first identified for testing. They would also permit a comparison of the structural response of panels with and without the additional thickness at certain locations.

Panel 6 tests demonstrated the complex system response to impacts. While the initial focus of the investigation had been on single panel response, early results from the tests with fiberglass panels hinted at “boundary condition” effects. Instruments measured high stresses through panels 6, 7, and 8. With this in mind, as well as forensic and sensor evidence that panel 8 was the likeliest location of the foam strike, the Board decided that the second RCC test should target panel 8, which was placed in an assembly that included RCC panels 9 and 10 to provide high fidelity boundary conditions. The decision to impact test RCC panel 8 was complicated by the lack of spare RCC components.

The specific RCC panel assemblies selected for testing had flight histories similar to that of STS-107, which was *Columbia’s* 28th flight. Panel 6 had flown 30 missions on *Discovery*, and Panel 8 had flown 26 missions on *Atlantis*.

### Test Projectile

The preparation of BX-250 foam test projectiles used the same material and preparation processes that produced the foam bipod ramp. Foam was selected as the projectile material because foam was the most likely debris, and materials other than foam would represent a greater threat.



Figure 3.8-3. A typical foam projectile, which has marks for determining position and velocity as well as blacked outlines for indicating the impact footprint.

The testing required a projectile (see Figure 3.8-3) made from standard stock, so investigators selected a rectangular cross-section of 11.5 by 5.5 inches, which was within 15 percent of the footprint of the mean debris size initially estimated by image analysis. To account for the foam's density, the projectile length was cut to weigh 1.67 pounds, a figure determined by image and transport analysis to best represent the STS-107 projectile. For foam with a density of 2.4 pounds per cubic foot,<sup>15</sup> the projectile dimensions were 19 inches by 11.5 inches by 5.5 inches.

### Impact Angles

The precise impact location of the foam determined the impact angle because the debris was moving almost parallel to the Orbiter's fuselage at impact. Tile areas would have been hit at very small angles (approximately five degrees), but the curvature of the leading edge created angles closer to 20 degrees (see Figure 3.4-4).

The foam that struck *Columbia* on January 16, 2003, had both a translational speed and a rotational speed relative to the Orbiter. The translational velocity was easily replicated by adjusting the gas pressure in the gun. The rotational energy could be calculated, but the impact force depends on the material composition and properties of the impacting body and how the rotating body struck the wing. Because the details of the foam contact were not available from any visual evidence, analysis estimated the increase in impact energy that would be imparted by the rotation. These analyses resulted in a three-degree increase in the angle at which the foam test projectile would hit the test panel.<sup>16</sup>

The "clocking angle" was an additional consideration. As shown in Figure 3.8-4, the gun barrel could be rotated to change the impact point of the foam projectile on the leading edge. Investigators conducted experiments to determine if the corner of the foam block or the full edge would impart a

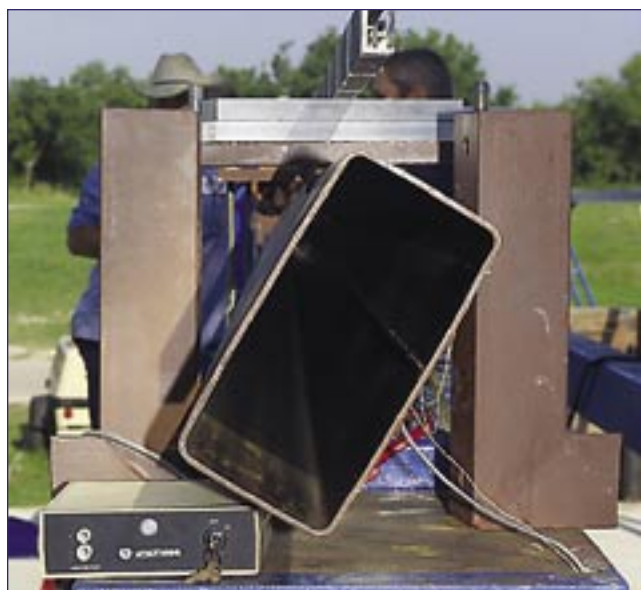


Figure 3.8-4. The barrel on the nitrogen gun could be rotated to adjust the impact point of the foam projectile.

greater force. During the fiberglass tests, it was found that a clocking angle of 30 degrees allowed the 11.5-inch-edge to fully contact the panel at impact, resulting in a greater local force than a zero degree angle, which was achieved with the barrel aligned vertically. A zero-degree angle was used for the test on RCC panel 6, and a 30-degree angle was used for RCC panel 8.

### Test Results from Fiberglass Panel Tests 1-5

Five engineering tests on fiberglass panels (see Figure 3.8-5) established the test parameters of the impact tests on RCC panels. Details of the fiberglass tests are in Appendix D.12.



Figure 3.8-5. A typical foam strike leaves impact streaks, and the foam projectile breaks into shards and larger pieces. Here the foam is striking Panel 6 on a fiberglass test article.

### Test Results from Reinforced Carbon-Carbon Panel 6 (From Discovery)

RCC panel 6 was tested first to begin to establish RCC impact response, although by the time of the test, other data had indicated that RCC panel 8-left was the most likely site of the breach. RCC panel 6 was impacted using the same parameters as the test on fiberglass panel 6 and developed a 5.5-inch crack on the outboard end of the panel that extended through the rib (see Figure 3.8-6). There was also a crack through the "web" of the T-seal between panels 6 and 7 (see Figure 3.8-7). As in the fiberglass test, the foam block deflected, or moved, the face of the RCC panel, creating a slit between the panel and the adjacent T-seal, which ripped the projectile and stuffed pieces of foam into the slit (see Figure 3.8-8). The panel rib failed at lower stresses than predicted, and the T-seal failed closer to predictions, but overall, the stress pattern was similar to what was predicted, demonstrating the need to incorporate more complete RCC failure criteria in the computational models.

Without further crack growth, the specific structural damage this test produced would probably not have allowed enough superheated air to penetrate the wing during re-entry to cause serious damage. However, the test did demonstrate that a foam impact representative of the debris strike at 81.9 seconds after launch could damage an RCC panel. Note that



Figure 3.8-6. A 5.5-inch crack on the outboard portion of RCC Panel 6 during testing.

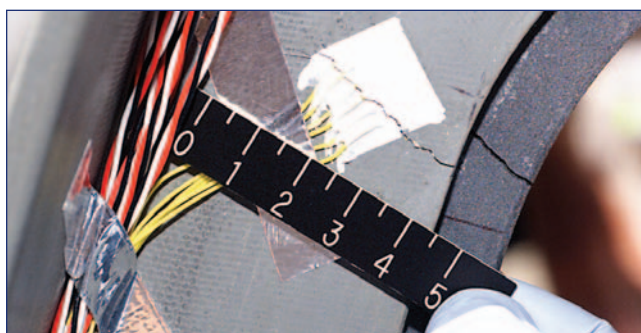


Figure 3.8-7. Two views of the crack in the T-seal between RCC Panels 6 and 7.

the RCC panel 6-left test used fiberglass panels and T-seals in panel 7, 8, 9, and 10 locations. As seen later in the RCC panel 8-left test, this test configuration may not have adequately reproduced the flight configuration. Testing of a full RCC panel 6, 7, and 8 configuration might have resulted in more severe damage.

#### Test Results from Reinforced Carbon-Carbon Panel 8 (From *Atlantis*)

The second impact test of RCC material used panel 8 from *Atlantis*, which had flown 26 missions. Based on forensic evidence, sensor data, and aerothermal studies, panel 8 was considered the most likely point of the foam debris impact on *Columbia*.

Based on the system response of the leading edge in the fiberglass and RCC panel 6 impact tests, the adjacent RCC panel assemblies (9 and 10) were also flown hardware. The reference 1.67-pound foam test projectile impacted panel 8

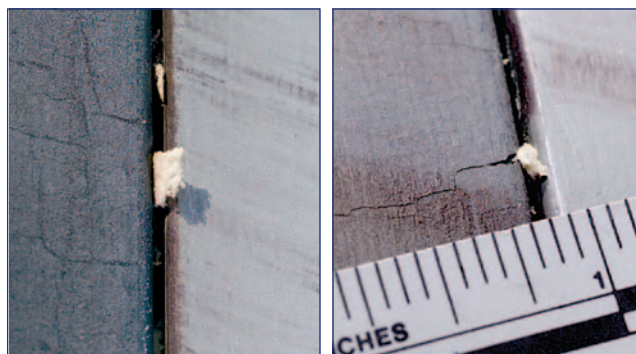


Figure 3.8-8. Two views of foam lodged into the slit during tests.



Figure 3.8-9. The large impact hole in Panel 8 from the final test.



Figure 3.8-10. Numerous cracks were also noted in RCC Panel 8.

at 777 feet per second with a clocking angle of 30 degrees and an angle of incidence of 25.1 degrees.

The impact created a hole roughly 16 inches by 17 inches, which was within the range consistent with all the findings of the investigation (see Figure 3.8-9). Additionally, cracks in the panel ranged up to 11 inches in length (Figure 3.8-10). The T-seal between panels 8 and 9 also failed at the lower outboard mounting lug.

Three large pieces of the broken panel face sheet (see Figure 3.8-11) were retained within the wing. The two largest pieces had surface areas of 86 and 75 square inches. While this test cannot exactly duplicate the damage *Columbia* incurred, pieces such as these could have remained in the wing cavity for some time, and could then have floated out of the damaged wing while the Orbiter was maneuvering in space. This scenario is consistent with the event observed on Flight Day 2 (see Section 3.5).

The test clearly demonstrated that a foam impact of the type *Columbia* sustained could seriously breach the Wing Leading Edge Structural Subsystem.

### Conclusion

At the beginning of this chapter, the Board stated that the physical cause of the accident was a breach in the Thermal Protection System on the leading edge of the left wing. The breach was initiated by a piece of foam that separated from the left bipod ramp of the External Tank and struck the wing in the vicinity of the lower half of the Reinforced Carbon-Carbon (RCC) panel 8.

The conclusion that foam separated from the External Tank bipod ramp and struck the wing in the vicinity of panel 8 is documented by photographic evidence (Section 3.4). Sensor data and the aerodynamic and thermodynamic analyses (Section 3.6) based on that data led to the determination that the breach was in the vicinity of panel 8 and also accounted for the subsequent melting of the supporting structure, the spar, and the wiring behind the spar that occurred behind panel 8. The detailed examination of the debris (Section 3.7) also pointed to panel 8 as the breach site. The impact tests (Section 3.8) established that foam can breach the RCC, and also counteracted the lingering denial or discounting of the analytic evidence. Based on this evidence, the Board concluded that panel 8 was the site of the foam strike to *Columbia* during the liftoff of STS-107 on January 23, 2003.

### Findings:

- F3.8-1 The impact test program demonstrated that foam can cause a wide range of impact damage, from cracks to a 16- by 17-inch hole.
- F3.8-2 The wing leading edge Reinforced Carbon-Carbon composite material and associated support hardware are remarkably tough and have impact capabilities that far exceed the minimal impact resistance specified in their original design requirements. Nevertheless, these tests demonstrate that this inherent toughness can be exceeded by

impacts representative of those that occurred during *Columbia's* ascent.

- F3.8-3 The response of the wing leading edge to impacts is complex and can vary greatly, depending on the location of the impact, projectile mass, orientation, composition, and the material properties of the panel assembly, making analytic predictions of damage to RCC assemblies a challenge.<sup>17</sup>
- F3.8-4 Testing indicates the RCC panels and T-seals have much higher impact resistance than the design specifications call for.
- F3.8-5 NASA has an inadequate number of spare Reinforced Carbon-Carbon panel assemblies.
- F3.8-6 NASA's current tools, including the Crater model, are inadequate to evaluate Orbiter Thermal Protection System damage from debris impacts during pre-launch, on-orbit, and post-launch activity.
- F3.8-7 The bipod ramp foam debris critically damaged the leading edge of *Columbia's* left wing.

### Recommendations:

- R3.8-1 Obtain sufficient spare Reinforced Carbon-Carbon panel assemblies and associated support components to ensure that decisions related to Reinforced Carbon-Carbon maintenance are made on the basis of component specifications, free of external pressures relating to schedules, costs, or other considerations.
- R3.8-2 Develop, validate, and maintain physics-based computer models to evaluate Thermal Protection System damage from debris impacts. These tools should provide realistic and timely estimates of any impact damage from possible debris from any source that may ultimately impact the Orbiter. Establish impact damage thresholds that trigger responsive corrective action, such as on-orbit inspection and repair, when indicated.

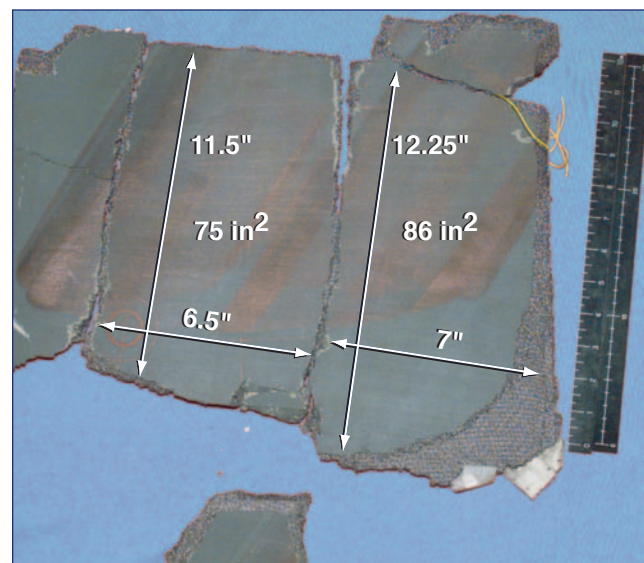


Figure 3.8-11. Three large pieces of debris from the panel face sheet were lodged within the hollow area behind the RCC panel.

## ENDNOTES FOR CHAPTER 3

The citations that contain a reference to "CAIB document" with CAB or CTF followed by seven to eleven digits, such as CAB001-0010, refer to a document in the Columbia Accident Investigation Board database maintained by the Department of Justice and archived at the National Archives.

- <sup>1</sup> See Dennis R. Jenkins, *Space Shuttle: The History of the National Space Transportation System – The First 100 Missions* (Cape Canaveral, FL, Specialty Press, 2001), pp. 421-424 for a complete description of the External Tank.
- <sup>2</sup> Scotty Sparks and Lee Foster, "ET Cryoinsulation," CAIB Public Hearing, April 7, 2003. CAIB document CAB017-03140371.
- <sup>3</sup> Scotty Sparks and Steve Holmes, Presentation to the CAIB, March 27, 2003, CAIB document CTF036-02000200.
- <sup>4</sup> See the CAIB/NAIT Joint Working Scenario in Appendix D.7 of Volume II of this report.
- <sup>5</sup> Boeing Specification MJ070-0001-1E, "Orbiter End Item Specification for the Space Shuttle Systems, Part 1, Performance and Design Requirements, November 7, 2002.
- <sup>6</sup> *Ibid.*, Paragraph 3.3.1.8.16.
- <sup>7</sup> NSTS-08171, "Operations and Maintenance Requirements and Specifications Document (OMRSD)" File II, Volume 3. CAIB document CAB033-12821997.
- <sup>8</sup> Dr. Gregory J. Byrne and Dr. Cynthia A. Evans, "STS-107 Image Analysis Team Final Report in Support of the Columbia Accident Investigation," NSTS-37384, June 2003. CAIB document CTF076-15511657. See Appendix E.2 for a copy of the report.
- <sup>9</sup> R. J. Gomex et al, "STS-107 Foam Transport Final Report," NSNS-60506, August 2003.
- <sup>10</sup> This section based on information from the following reports: MIT Lincoln Laboratory "Report on Flight Day 2 Object Analysis;" Dr. Brian M. Kent, Dr. Kueichien C. Hill, and Captain John Gulick, "An Assessment of Potential Material Candidates for the 'Flight Day 2' Radar Object Observed During the NASA Mission STS-107 (Columbia)", Air Force Research Laboratory Final Summary Report AFRL-SNS-2003-001, July 20, 2003 (see Appendix E.2); Multiple briefings to the CAIB from Dr. Brian M. Kent, AFRL/SN (CAIB document CTF076-19782017); Briefing to the CAIB from HQ AFSPC/XPY, April 18, 2003 (CAIB document CAB066-13771388).
- <sup>11</sup> The water tanks from below the mid-deck floor, along with both Forward Reaction Control System propellant tanks were recovered in good condition.
- <sup>12</sup> *Enterprise* was used for the initial Approach and Landing Tests and ground tests of the Orbiter, but was never used for orbital tests. The vehicle is now held by the National Air and Space Museum. See Jenkins, *Space Shuttle*, pp. 205-223, for more information on *Enterprise*.
- <sup>13</sup> Philip Kopfinger and Wanda Sigur, "Impact Test Results of BX-250 In Support of the Columbia Accident Investigation," ETP-MS-03-021, July 17, 2003.
- <sup>14</sup> Details of the test instrumentation are in Appendix D.12.
- <sup>15</sup> Evaluations of the adjustments in the angle of incidence to account for rotation are in Appendix D.12.
- <sup>16</sup> The potential damage estimates had great uncertainty because the database of bending, tension, crushing, and other measures of failure were incomplete, particularly for RCC material.